mps1 and mad mutations reduce Cryptococcus neoformans titan cell viability

mps1 and *mad* mutations reduce *Cryptococcus neoformans* titan cell viability

Koly Aktar, Thomas Davies*, Ioanna Leontiou*, Ivan Clark, Christos Spanos, Edward Wallace, Laura Tuck, A. Arockia Jeyaprakash and Kevin G. Hardwick#

Institute of Cell Biology, School of Biological Sciences, University of Edinburgh

corresponding author
* equal contribution

Abstract

Cryptococcus neoformans is an opportunistic, human fungal pathogen which undergoes fascinating switches in cell cycle control and ploidy when it encounters stressful environments such as the human lung. Here we carry out a mechanistic analysis of the spindle assembly checkpoint (SAC) which regulates the metaphase to anaphase transition, focusing on Mps1 kinase and the downstream checkpoint components Mad1 and Mad2. We demonstrate that *Cryptococcus mad1Δ* or *mad2Δ* strains are unable to respond to microtubule perturbations, continuing to re-bud and divide, and die rapidly as a consequence. Fluorescent tagging of Chromosome 3, using a lacO array and mNeonGreen-lacI fusion protein, demonstrates that *mad* mutants are unable to maintain sister-chromatid cohesion in the absence of microtubule polymers. Thus, the classic checkpoint functions of the SAC are conserved in *Cryptococcus*. In interphase, GFP-Mad1 is enriched at the nuclear periphery, and it is recruited to unattached kinetochores in mitosis. Purification of GFP-Mad1 followed by mass spectrometric analysis of associated proteins show that that it forms a complex with Mad2 and that it interacts with other checkpoint signalling components (Bub1) and effectors (Cdc20 and APC/C sub-units) in mitosis. We also demonstrate that overexpression of Mps1 kinase is sufficient to arrest *Cryptococcus* cells in mitosis, and show that this arrest is dependent on both Mad1 and Mad2. We find that a C-terminal fragment of Mad1 is an effective *in vitro* substrate for

Mps1 kinase and map several Mad1 phosphorylation sites. Some sites are highly conserved within the C-terminal Mad1 structure and we demonstrate that mutation of threonine 667 (T667A) leads to loss of checkpoint signalling and abrogation of the *GAL-MPS1* arrest. Thus Mps1-dependent phosphorylation of C-terminal Mad1 residues is a critical step in *Cryptococcus* spindle checkpoint signalling. Finally, we analyse the phenotype of *mad* and *mps1* mutants during titan cell generation: quantitating viability of titan cells and their daughters generated during the ensuing reductive division. The *mad1Δ, mad2Δ* and *mps1Δ* mutants show significantly reduced viability: many titans are dead and others produce slow growing colonies. We propose that these *Cryptococcus neoformans* checkpoint proteins have important roles in ensuring high fidelity chromosome segregation during stressful conditions, such that those heightened during its polyploid infection cycle.

Introduction

Cryptococcus neoformans is an important human fungal pathogen [1], responsible for the death of around 20% of AIDS patients. Recent estimates have 152,000 annual cases of *Cryptococcal* meningitis worldwide, mainly in Sub-Saharan Africa, leading to ~112,000 deaths in AIDS patients [2]. Few drugs are currently available and drug-resistant strains have emerged in the clinic, so new treatments are urgently required [3]. We are investigating mitotic control of chromosome segregation as a possible future drug target in *Cryptococcus neoformans* [4].

Important previous studies have described cell division in this basidiomycete. It has 14 chromosomes, and undergoes a partially open mitosis with the nuclear division taking place in the bud and one set of chromosomes moving back to the mother cell during anaphase [5]. During human infection *Cryptococcal* cells are stressed and undergo a fascinating morphological transition, forming polyploid titan cells in the lung [6]. These large cells (up to 100 micron diameter) are protective: the immune system struggles to clear them because of their size and their protective outer capsule [7]. These titan cells are polyploid and a recent study identified a specific Cyclin, Cln1, as a key regulator of this transition [8]. Polyploidisation takes place after a G2 arrest and involves endo-reduplication. Once formed, titan cells continue to divide by budding off small daughter cells, which have a high viability and are haploid. How this reductive division, from polyploid titan to haploid daughter, is achieved is completely unknown. It has been proposed that this division is likely to be somewhat error-prone, leading to aneuploid daughters. Such aneuploidy would increase genetic diversity in the fungal population and thus relevant to the generation of drug-resistance in the clinic [4].

The spindle assembly checkpoint (SAC) is a key regulator of mitotic and meiotic divisions, and has been studied in detail in several model systems and human cells [9] [10]. This cell cycle checkpoint monitors interactions between kinetochores and spindle microtubules, and if any problems are apparent the SAC provides additional time for them to be resolved, by delaying the metaphase to anaphase transition. Its molecular components were identified in budding yeast genetic screens [11-13], and the *MAD*, *BUB* and *MPS1* genes and their mode of action have been found to be extremely well conserved through eukaryotic evolution [14]. The SAC pathway has not yet been described in *Cryptococcus*, although both the *BUB1* and *MPS1* kinases were shown to be relevant to virulence in a genome-wide screen where 129 protein kinases were knocked out [15].

Here we have knocked out the *MAD1* and *MAD2* genes and compared their phenotypes to that of the *mps1Δ* strain. We demonstrate that all three components are essential for SAC function: in response to anti-microtubule drug treatment, deletion mutants are unable to maintain sister-chromatid cohesion and continue to divide. Overexpression of CnMps1 kinase is sufficient to induce metaphase arrest and this is dependent on both Mad1 and Mad2. We identify Mps1 phosphorylation sites in the Mad1 C-terminus and demonstrate that the C-terminal Mad1 T667A substitution abolishes SAC signalling and *GAL-MPS1* arrest. Finally, we show that whilst the *mad* and *mps1* mutants can form titan cells, they display significantly reduced viability. Thus, SAC components have important roles to play in ensuring high fidelity chromosome segregation, not only in yeast but also in titan cell divisions.

Results

Analysis of the *Cryptococcus neoformans* genome sequence in the FungiDB database identified CNAG_04824 and CNAG_01638 as likely homologues of *MAD1* and *MAD2*. Their sequences are well conserved, with CnMad1 being predicted to be an elongated coiled-coil protein, likely to bind both Mad2 and Bub1 (Fig.1A). To test whether their function is conserved we knocked out both genes, using the *amdS* Blaster (dominant recyclable marker) approach, developed in *Cryptococcus* by James Fraser et al [16]. First we replaced the *MAD* gene with the *amdS* marker by homologous recombination (Fig.1B). *AmdS,* encoding the *Aspergillus nidulans* acetamidase gene*,* enables acetamide to be used as both a carbon and nitrogen source by cells, and transformants were selected for on acetamide plates. In a second step the *amdS* marker was allowed to recombine out, via flanking repeat sequences, and its loss was selected for by growth on fluoracetamide. This compound kills any cells still containing the *amdS* marker as it is metabolised into toxic fluoroacetyl CoA and fluorocitrate, disabling aconitase and inhibiting the citric acid cycle. To help confirm the *mad1* deletion, we made a polyclonal anti-Mad1 antibody by expressing amino acids 1-200 of Mad1 fused to 6xHis-MBP (maltose binding protein) in bacteria and injecting the purified MBP-Mad1 protein as antigen into a sheep. The anti-Mad1 immunoblot data in Fig.1C confirms that the correct gene had been knocked out and that Mad1p is no longer expressed.

To analyse the loss of function phenotype we plated the *mad1*Δ on the anti-microtubule drug benomyl. Fig.1D shows that the *mad1*Δ strain is sensitive to this anti-MT drug. We used *mps1Δ* as a control: this strain has been previously described by the Bahn group when analysing the kinome of *Cryptococcus neoformans* [15]. Fig.1D shows that we can rescue the benomyl sensitivity of the *mad1*Δ strain by complementation with a GFP-Mad1 construct, confirming that we have knocked out the right gene and that the benomyl sensitivity observed is due to loss of Mad1 function.

Next we knocked out the *MAD2* gene using the same approach, and confirmed homologous recombination through PCR analysis of genomic DNA, before and after the *amdS* marker was lost (Fig.2A,B). These strains were also found to be benomyl sensitive and could be rescued by expression of an ectopic copy of Myc-*MAD2* expressed from the *GAL7* promoter in galactose media (Fig.2C).

We next made a *mad1, mad2* double mutant, by repeating this experiment and sequentially knocking out *MAD2* in the *mad1Δ* strain. Fig.2D shows that the double

mutant (*mad1, mad2*) was no more sensitive than the single mutants, suggesting that these proteins carry out their function(s) in a concerted fashion. This is consistent with known behaviour of these Mad proteins in other systems where they form a stable, constitutive complex [17-19] [20].

As expected [21], the strain lacking Mps1 protein kinase is significantly more sensitive to the anti-microtubule drugs than the *mad* mutants (see Fig.2D). Our interpretation is that CnMps1 kinase is likely to have other mitotic functions, in addition to checkpoint signalling, such as error-correction and bi-orientation [22-24]. *mps1Δ* mutants were also reported to be temperature sensitive. We found a subtle temperature-sensitive phenotype on plates for the *mad* mutants (Fig.2D), and Fig.2E shows that growth of liquid cultures in a plate reader confirms the phenotype at 37°C for both *mad1* and *mad2* mutants. This *ts* phenotype was not as severe as that displayed by the *mps1Δ* mutant. Thus, as expected of a SAC component, the *mad1* and *mad2* mutants are sensitive to anti-microtubule drugs. However, they are also sensitive to other stresses, such as high temperatures, which to our knowledge has not been reported in other yeasts.

mad1Δ and *mad2Δ* mutants are checkpoint defective

To test whether these mutants have SAC defects, we carried out additional assays that analyse how individual cells respond to anti-microtubule drug treatment. More specifically, we asked whether they can arrest in mitosis and maintain sister-chromatid cohesion when treated with the microtubule-depolymerising agent nocodazole. Fig.3A&B reveal that, unlike wild-type (H99) cells, *mad1Δ*, *mad2Δ,* or *mps1Δ* mutants were unable to arrest as large-budded cells when treated with nocodazole. Wild-type cells display a very robust arrest under these conditions (2μg/ml nocodazole treatment for 90 minutes at 30°C). A subtle mitotic delay, in response to nocodazole treatment, might be missed with such fixed time point analysis, so we also employed microfluidics to analyse in more detail how single cells respond to nocodazole over time. Strains were pre-grown in SC media and then put in the microfluidics device, where single cells were captured (Fig.3C) before imaging. After 5 hours, nocodazole was added (2μg/ml) and imaging continued for a further 6 hours, with images being captured every 2 minutes. Movies were then analysed to see how many individual cells arrested in the nocodazole, and how many continued to re-bud and divide. Fig.3D confirms that the *mad1Δ*, *mad2Δ,* and *mps1Δ* mutants were all unable to delay mitotic progression in response to nocodazole treatment. We conclude that

deletion of any one of these genes has likely completely abrogated the SAC. The Sanyal lab independently generated a *mad2Δ* strain and demonstrated that it was unable to arrest as large-budded cells upon thiabendazole treatment [25].

The key roles of the SAC are to delay the metaphase to anaphase transition and to protect sister-chromatid cohesion. If sister-chromatids separate prematurely, before bi-orientation of all chromosomes is complete, then sisters will mis-segregate randomly leading to aneuploidy. GFP-marked chromosomes are widely used in model organisms to monitor and quantitate sister-chromatid separation [26] [27]. We integrated an array of 240 lac operators (lacO, [28]) into chromosome 3 and expressed a lacI-NeonGreen fusion protein to mark just one of the fourteen *Cryptococcus* chromosomes (Fig. 4A). We knocked out *MAD2* in this strain as above (producing KA159) and complemented that strain with an ectopic copy of *MAD2* (producing KA196). Comparison of these strains in the presence of nocodazole demonstrates the expected sister-chromatid cohesion defect in the *mad2Δ* strain (Fig.4B). After 90 minutes of nocodazole treatment ~40% of *mad2Δ* cells have separated sisters, compared to only 2% of wild-type cells in (Fig.4C). It should be noted that in this assay not all sisters will visibly separate, as in the absence of microtubules there are no spindle forces pulling them apart.

Next, we analysed the rate of death of the *mad* mutants in response to anti-microtubule drug treatment. To quantitate this, we determined the number of colony forming units (CFU) on plates following nocodazole treatment of wild-type and *sac*- mutant cultures. The *mad* and *mps1* mutants all display a rapid rate of death (SFig.1).

In summary, in response to anti-microtubule drug treatments, the *mad* mutants fail to arrest, fail to maintain sister-chromatid cohesion, re-bud and die.

Mad1 localises to the nuclear envelope and is recruited to unattached mitotic kinetochores

In many systems the Mad proteins interact with the nuclear periphery throughout interphase and only get recruited to unattached kinetochores during mitosis [19, 29-32]. Several reasons for this have been suggested, including that by keeping the Mad proteins away from the Bub proteins, which decorate chromosomes, it may prevent premature checkpoint signalling. Very early in vertebrate mitosis, before mitotic kinetochores have matured enough to be active in checkpoint signalling, nuclear pores act as a site of MCC assembly and thereby prevent premature anaphase onset [31]. Transport related

functions at the nuclear envelope have been proposed for the Mad1 protein in *S.cerevisiae* [33]. We analysed GFP-CnMad1 through the cell cycle and carried out double label experiments with γ-tubulin and kinetochore markers (mCherry-Dad2 and CENP-A, mCherry-Cse4). Fig.5 shows that when the checkpoint isn't active GFP-Mad1 is enriched at the nuclear periphery. Representative mitotic images demonstrate that GFP-Mad1 is recruited to unattached kinetochores during mitosis and enriched there during SAC (nocodazole) arrest (Fig.5DE). During a SAC-dependent mitotic arrest, GFP-Mad1 co-localises with kinetochore markers, such as Cse4 and Dad2. Although close to spindle poles, Mad1 does not co-localise with gamma-tubulin (Fig.5BC). All of this is consistent with GFP-Mad1 being recruited to unattached mitotic kinetochores in *Cryptococcus neoformans*.

Mad1 interacts with several checkpoint components and effectors

To understand more about the molecular interactors of GFP-Mad1 in *Cryptococcus neoformans* we carried out large scale purifications, from cycling and from checkpoint arrested cells. We grew 500mls of yeast in YPD, added nocodazole for 3 hours, then harvested cells, made whole cell extracts and immunopurified GFP-Mad1 using GFP-TRAP beads. After careful washing and elution, Mad1 and its interacting partners were analysed by mass spectrometry. The volcano plots in Fig.6A, comparing tagged with an untagged control, demonstrate that Mad1 specifically interacts with other SAC components (Mad2, Bub1, Bub3, Mps1) and effectors (Cdc20 [34, 35]). In mitotic extracts, CnMad1 interacts very significantly with both Mad2 and Bub1, along with other checkpoint proteins Bub3 and Mps1, and the effectors Cdc20 and APC/C sub-units (Apc1,2,3,4,5,6,8 [36]). Other interacting partners include key mitotic regulators, Plk1 (Polo kinase) and PP1 (Protein Phosphatase 1) (Fig.6B). In cycling cells, Mad1 interacted with several nucleoporins including the TPR/Mlp homologue (Fig.6C). Live cell imaging (Fig.6D) confirms that GFP-Mad1 and mCherry-Bub1 co-localised at unattached kinetochores, in nocodazole-arrested cells. Analysis of the Mad1 protein sequence (Fig.1A) identified two RLK motifs that might drive its interaction with Bub1 [37-39]. We made point mutations in both RLK motifs of GFP-Mad1 and tested whether mutant alleles were still able to rescue *mad1Δ.* Fig. 6E shows that *mad1-rlk-AAA* (mutating the conserved RLK residues 567-569) mutant was unable to rescue the benomyl sensitivity of *mad1Δ*, confirming that the Bub1 interaction is important for Mad1 checkpoint signalling functions in *Cryptococcus*.

Mutation of nearby RLK residues (549-551) that are not conserved had no impact on function. We tested Mad1-Bub1 complex formation by co-immunoprecipitation. Fig.6F demonstrates that whilst wild-type GFP-Mad1 co-immunoprecipitates with mCherry-Bub1 in mitotic extracts, the GFP-*mad1-rlk(567-569)* mutant does not. We conclude that the key signalling interaction between Bub1 and Mad1 is conserved in *Cryptococcus*.

CnMps1 overexpression activates the checkpoint, arresting cells in mitosis in a Mad1 and Mad2-dependent fashion

In several systems, overexpression of Mps1 kinase is sufficient to activate checkpoint signalling and arrest cells in early mitosis [40] [41]. Sometimes it does this without significantly perturbing the mitotic machinery and cells simply divide at a slow rate due to a prolonged mitotic delay each cell cycle [40]. This has been a very useful tool in other systems, so we assembled a P_{GAL7}-*MPS1* (Myc-tagged) construct that does not express in YPD (glucose media) but expresses Mps1 at high levels after galactose addition (see Fig.7A immunoblot time course). This strain also expresses GFP-tubulin and analysis of cultures demonstrated a very robust metaphase arrest with 60% short mitotic spindles 3 hours after addition of 2% galactose, and >80% arrest after 5 hours. Carrying out the same experiment in *mad1*Δ or *mad2*Δ cells led to ~20% mitotic cells, demonstrating that the P_{GAL7}-*MPS1* induced checkpoint arrest is dependent on both Mad1 and Mad2. We were surprised to observe that all of these strains (wild-type, *mad1*Δ and *mad2*Δ) died quickly after galactose addition (data not shown). Future experiments will be needed to understand what kills these cells. Intriguingly, we also found that overexpression of kinase-dead Mps1 was also very toxic.

The Mad1 C-terminus is phosphorylated by Mps1 and this stabilises its interaction with Cdc20

Mad1 is an important Mps1 substrate for SAC signalling [40, 42]. To test whether Mad1 is phospho-regulated in *Cryptococcus*, we carried out *in vitro* Mps1 kinase assays. The CnMps1 kinase domain was expressed and purified as a 6xHis-Sumo-tagged fusion protein (residues 478-842) from bacteria. Radioactive assays employing this recombinant kinase show that the Mad1 C-terminus (Mad1-CT) is a good Mps1 substrate (Fig.8A). Mass spectrometric analysis identified 8 Mad1 phospho-peptides and T667/668 and T660/661 as candidate phosphorylation sites (Fig.8B&C). Alphafold modelling suggests

that CnMad1 T667/T668 could be equivalent to T716 in human Mad1, previously shown to be important for Cdc20 interaction and checkpoint signalling [42]. We made alanine substitutions in T660, T661, T667 and T668 and found that the mutation T667A leads to a strong benomyl-sensitive phenotype, much like the *mad1* deletion (Fig.8D).
Kinase assays with the double TT667/668AA *mad1* mutant confirm that these are significant *in vitro* phosphorylation sites (exhibiting a 30% reduction in ^{32}P incorporation). The *mad1-T667A* point mutant was unable to arrest in nocodazole (Fig.8F) and when P_{GAL7}*-MPS1* was overexpressed in galactose (Fig.8G). We conclude that the C-terminal phosphorylation site T667 is an important Mps1 substrate in *C. neoformans*. Similar Mad1 phosphorylation enhances a Mad1-Cdc20 interaction in humans [42], but our preliminary *in vitro* studies using recombinant proteins have as yet failed to demonstrate a similar phospho-dependent interaction between the N-terminus of Cdc20 and the C-terminus of Mad1 in *Cryptococcus*.

*mps1*Δ*, mad1*Δ *and mad2*Δ *titan cells have reduced viability, but this is not due to their defective SAC*

During infection cryptococcal cells become stressed and form polyploid titan cells [6], to protect themselves from macrophages in the immune system [7]. Titans can be generated in the lab [43-45] by starving yeast overnight and then mimicking the conditions of the human lung (e.g. 37°C, 5% CO_2, 10% serum/PBS). After 3 days ~20% of the population become polyploid titan cells [43].
We were very interested to test whether the *MAD* and *MPS1* genes were required to maintain viability of *Cryptococcus* titan cells. To do this, we used the *in vitro* titanisation assay developed by Liz Ballou [43]. We found that all the *mad* and *mps1* deletion strains could make titan cells and used india-ink staining of their capsules to measure titan cell size (Fig.9A). We then micro-dissected >100 individual titans for each strain to test their viability. Fig.9B shows that almost all the wild-type titans form viable colonies, when placed on rich growth media (YPDA plates) and allowed to grow at 30°C for 2-3 days. The same experiment reveals that only ~50% of *mps1* mutant titan cells were viable and around ~70% of the *mad1* and *mad2* mutant titans. Of those titans that were able to produce viable colonies, several of the *mps1*, *mad1* and *mad2* mutant colonies were slow growing compared to the wild-type (Fig.9C). We are currently testing whether some of these slow-growing colonies contain aneuploid cells. This indicates that the viability of

titan cells is severely compromised by mutations in SAC genes. However, when we tested specific alleles of SAC genes (*bub1-cd1* [46] and *mad1-667A*), rather than null mutants, we found that their viability was not compromised even though these alleles are checkpoint defective. Our interpretation of this experiment is that a sub-set of the checkpoint proteins (Mad1, Mad2 and particularly Mps1 kinase) have a novel function that is particularly important for the viability of titan cells and/or their daughters.

Discussion

The spindle assembly checkpoint (SAC) has not previously been analysed in mechanistic detail in basidiomycetes. Here we have demonstrated that the checkpoint signalling roles of Mps1 kinase, Mad1 and Mad2 and their molecular interactions are very well conserved in *Cryptococcus neoformans*. In a second study, we demonstrated that Bub1 and Bub3 functions are also very well conserved [46]. One important difference in the SAC is that *Cryptococcus* lacks a BubR1/Mad3 gene as, unlike in humans, *S.cerevisiae* and *S.pombe*, the CnBub1 gene hasn't undergone duplication and CnBub1 carries out the functions of both Bub1 (as a kinetochore-bound SAC signalling scaffold) and Mad3 (as part of the diffusible APC/C inhibitor) [46]. Here we have also shown that Mps1 phospho-regulation of Mad1 is conserved in *Cryptococcus*. Thus, much of what we know about SAC signalling, from the past 30 years of studying model systems, is likely relevant in this important human fungal pathogen. We hope that this will enable us to efficiently identify specific SAC inhibitors and employ them in clinical treatments, in combination treatment with anti-microtubule drugs [47].

In interphase cells CnMad1 can be imaged at the nuclear periphery (Fig.5) and mass-spectrometric analysis of GFP-Mad1 pull downs identified several components of nuclear pores including the TPR/Mlp1 component of the inner basket. This TPR interaction is conserved but the role of Mad1-Mad2 localisation at the nuclear periphery remains unclear: it may keep Mad and Bub proteins apart in interphase to prevent inappropriate signalling, or the Mad proteins could have a transport-related function at the nuclear pore [19, 30] [33, 48]. In mitotic cells GFP-Mad1 was recruited to unattached kinetochores, co-localising with Bub1, Cse4 and Dad2 centromere/kinetochore markers (Fig.5). Mass-spec identified Mad2, Bub1, Bub3, Mps1, Cdc20, Apc1,2,3,4,5,6,8 and PP1 as mitotic interactors highlighting its role at the centre of SAC signalling alongside Bub1 (Fig.6).

We demonstrated that the *mad* and *mps1* mutants are unable to arrest cells at metaphase in response to anti-microtubule drug treatment (Fig.3) and have developed a sister-chromatid cohesion assay which demonstrates that Cn*mad* mutants are unable to maintain cohesion in nocodazole challenge (Fig.4). Thus these proteins all carry out critical SAC function(s). Specific alleles of CnMad1 were generated, demonstrating that Bub1 binding (RLK mutant) and Mps1-dependent phosphorylation (T667) are important for checkpoint signalling and SAC arrest.

Our analysis indicates that the *mad1, mad2* and *mps1* deletion mutants all have a temperature-sensitive phenotype (Fig.2). To our knowledge, this has not been reported for *mad* mutants in other systems. Whilst several *mps1-ts* alleles were described, that is because Mps1 kinase has an essential function in spindle pole body duplication in *S.cerevisiae* [13]. However, that function is not conserved in other systems [41, 49]. Growth at 37°C is very relevant to human infections and so we are keen to see what impact these *mad/mps1* mutations have in infection models. As a first step we generated titan cells *in vitro*, requiring growth at 37°C in 5%CO_2 and 10%FCS for 3 days. Fig.9 demonstrates that all the deletion strains have reduced titan cell viability but, importantly, that this is not due to loss of SAC signalling. Point mutations that abolish the SAC, such as *mad1-T667A* and *bub1-cd1* [46], did not display reduced titan cell viability. The simplest interpretation of this is that Mad1, Mad2 and Mps1 have an additional function(s) that is required for full viability of titan cells. Further studies are needed to determine this function, which appears to become more important during growth in stressful conditions. We are analysing spindle assembly and chromosome segregation to see if any errors can be detected during the slightly faster haploid cell divisions at 37°C.

The importance of *MAD1, MAD2* and *MPS1* in titan cells could be directly related to their increased ploidy. Genome-wide genetic screens in *S. cerevisiae* demonstrated that certain genes become more important with increased ploidy [50]. The major pathways identified with critical roles at higher ploidy were DNA recombination, sister-chromatid cohesion and kinetochore-microtubule attachments. In *S.cerevisiae* only one microtubule binds to each kinetochore [51]. One hypothesis proposed was that in *S. cerevisiae* tetraploid cells there is a high incidence of syntelic/monotelic chromosome attachments to spindle poles, and thus Sgo1 and error-correction activities of kinases such as Aurora B become essential for viability [50]. It is not known how many microtubules bind a single kinetochore in *Cryptococcus neoformans*, but as their centromeres are regional (20-100kb in size [52]) we suspect that it is more than one. Having multiple microtubule binding sites per kinetochore would mean that merotelic attachments (where single kinetochores attach inappropriately to microtubules from both spindle poles) are possible in polyploid titan cells. We propose that defective/inappropriate kinetochore attachments in polyploid titan cells are a cause of chromosome loss, aneuploidy and reduced viability. Reduced error-correction [23, 24] could explain the impact of the loss of Mps1 kinase in titan cells. Mad1 recruits a kinesin motor protein to kinetochores in fission yeast (Cut7) and humans (CENP-E) [53]. Whether this is the case in *Cryptococcus* remains to be seen, but it might explain

the reduced viability of *mad1* titan cells. Future studies on the roles of Mad, Bub and Mps1 proteins in titan cells will be fascinating.

Acknowlegements

We would like to thank all members of the Hardwick and JP labs for their support, discussions and suggestions on this manuscript; Paige Erpf and James Fraser for Safe Haven and Blaster constructs; Kaustuv Sanyal, Lukasz Kozubowski, Yong-Sun Bahn and Liz Ballou for *Cryptococcus neoformans* strains and plasmids; David Leach and Dave Sherratt for the lacO array; Ken Sawin for anti-mCherry antibodies; Connie Nichols for information on pCN19; Liz Ballou for many helpful *Cryptococcus* tips and suggestions; Dave Kelly, Toni McHugh and Dhanya Cheerambathur for help with microscopy and generating scripts and Peter Swain for leading on the ISSF funding (IC).

This work was supported by grants from the Leverhulme Trust (RPG-2018-379 to IL, KGH); the Darwin Trust of Edinburgh (KA, APS); the Wellcome Trust (SRF 202811 to AAJ; WCCB core grant 203149; iCM programme 218470 to TD, the Wellcome Trust-University of Edinburgh Institutional Strategic Support Fund, IC) and a Wellcome Sir Henry Dale Fellowship 208779/Z/17/Z to EW.

Materials and Methods

Yeast strains

Cryptococcus strains were all derived from *Cryptococcus neoformans* var. *grubii* H99.

Strains name	Genomic details
YSB3632	*mps1Δ::NAT* [Ref 13].
CNSD159	*TUB4::TUB4-mCherry:G418.* [Ref 22].
CNSD105	*DAD2::DAD2-mCherry:G418* [Ref 22].
KA43	*mad1Δ::amds*
KA51	*mad1Δ* (no selection, as *amds* recombined out)
KA53	*mad2Δ::amds*
KA55	*mad2Δ* (no selection, as *amds* recombined out)
KA28	*HISp:GFP-MAD1:HYG* (chrom 3, safe haven 3, pPEE37).
KA44	*mad1Δ, HISp:GFP-MAD1:HYG* (chrom 3, safe haven 3, pPEE37).
KA77	*mad1Δ*, *mad2Δ*
KA113	*mad2Δ, GALp-myc-MAD2:NAT* (chrom 14, safe haven 7, pPEE31)
IL08	*GALp-myc-MPS1:G418* (chrom 14, safe haven 7, pPEE36).
KA61	*mad1Δ*, *GALp-myc-MPS1:G418* (chrom 14, safe haven 7, pPEE36).
KA63	*mad2Δ*, *GALp-myc-MPS1:G418* (chrom 14, safe haven 7, pPEE36).
KA159	*HISp-mNeonGreen-lacI:G418* (chrom 14, safe haven 7, pPEE36), *lacO-array:HYG* (chrom 3, safe haven 3, pPEE37), *mad2Δ:amds.*
KA196	*HISp-mNeonGreen-lacI:G418* (chrom 14, safe haven 7, pPEE36), *lacO-array:HYG* (chrom 3, safe haven 3, pPEE37), *mad2Δ:amds, MAD2:NAT* (chrom 7, safe haven 5 pPEE29)
KA118	*DAD2::DAD2-mCherry:G418*, *mad1Δ, HISp:GFP-MAD1:HYG* (chrom 3, safe haven 3, pPEE37).
KA139	*TUB4::TUB4-mCherry:G418*, *mad1Δ*, *HISp:GFP-MAD1:HYG* (chrom 3, safe haven 3, pPEE37).
KA203	*Cse4::CSE4-mCherry:G418, mad1Δ*, *HISp:GFP-MAD1:HYG* (chrom 3, safe haven 3, pPEE37).
KA208	*HISp-mCherry-BUB1:NAT* (chrom 14, safe haven 7, pPEE31), *mad1Δ*, *HISp:GFP-MAD1:HYG* (chrom 3, safe haven 3, pPEE37).
KA163	*mad1Δ, HISp:GFP-Mad1-T667A:HYG* (chrom 3, safe haven 3, pPEE37).
KA172	*mad1Δ, HISp:GFP-Mad1-T668A:HYG* (chrom 3, safe haven 3, pPEE37).
KA177	*mad1Δ, HISp:GFP-Mad1-T661A:HYG* (chrom 3, safe haven 3, pPEE37).

Yeast media

All *Cryptococcus* strains were generated in the H99 genetic background and stored in YPDA (2% bactopeptone, 1% yeast extract, 2% glucose, 2% agar, 1mM adenine) with 50% glycerol at -80 ºC. Strains were grown on YPDA plates for two days prior to use. For

microfluidic experiments yeast synthetic complete media was used (SC: 0.67% Yeast Nitrogen Base; amino acid mix; 2% glucose). Knockout transformants generated using the blaster cassette were selected on plates containing YNB medium (0.45% yeast nitrogen base w/o amino acids and ammonium sulphate, 2% glucose, 10mM ammonium sulphate, 2% agar, 1mM adenine) with 5mM acetamide. To enable the blaster cassette to recombine out strains were streaked onto YPD twice and then YNB media containing 2% glucose, 10mM ammonium sulphate, and 10mM fluoroacetamide, as described previously[16]. For drug selection cells were grown on YPDA plates containing 300µg/ml hygromycin B (Invitrogen), 100µg/ml Geneticin (G418 Sulphate, Gibco) or 100µg/ml nourseothricin (Jena Bioscience). For expression from the *GAL7* promoter: it was switched on and off by adding 2% galactose or 2% glucose respectively.

Plate reader experiment (variable temperatures): log phase cells were diluted to OD 0.2 and grown for 20 hours in a Tecan i-control plate reader (infinite 200Pro), with time points taken every 10 minutes.

Gibson assembly, sequencing

Primers were purchased from either Sigma-Aldrich/Merck or IDT. Gibson assembly and NEBuilder® HiFi DNA assembly (New England Biolabs) were performed following manufacturer's instructions; sequencing was carried out using Big Dye.

Plasmids generated in this study:

KACP1 mad1 deletion: Bluescript-MAD1-5'UTR(1kb)_amds2_MAD1-3'UTR(1kb)
KACP2 mad2 deletion: Bluescript-MAD2-5'UTR(1kb)_amds2_MAD2-3'UTR(1kb)
KACP3 pPEE37:HISp-GFP-*MAD1*:hygR
KACP4 pPEE31:5'UTR(1kb)mCherry-*CSE4*:NatR
KACP5 pPEE37: 240xlacO-array:hygR
KACP6 pPEE36:Gpd1p_lacI-mNeonGreen:G418
KACP7 pPEE36:Gal7p_myc_*MPS1*:G418
KACP8 pPEE37:Gal7p_myc_*MAD2*:hygR
KACP9 pPEE37: HISp_GFP_*mad1_549RLK/AAA*:hygR
KACP10 pPEE37: HISp_GFP_*mad1-567RLK/AAA*:hygR
KACP11 pPEE37: HISp_GFP_*mad1T661A*:hygR
KACP12 pPEE37: HISp_GFP_*mad1T667A*:hygR
KACP13 pPEE37: HISp_GFP_*mad1T668A*:hygR

Primers used in this study:

Primer number	Primer name	Sequence	Purpose
KA 05	KH_CNY	5'_ ATGTATGCAAGATGTATGCG_3'	Safe haven 3
KA 07	HYG FORW 3	5'_CACTCGTCCGAGGGCAAAGG_3'	Safe haven 3 screen
KA95	M1D F1F	5'_Ctatagggcgaattggagctatttgatccaagacgggatc_3'	*mad1* D
KA96	M1D F1R	5'_ aatatagtggcatgattgaagaaagaggatatggagttgc_3'	*mad1* D
KA97	M1D F3F	5'_Gatggctagagtagaacttatacaatccaaatgtatatgtcg_3'	*mad1* D
KA98	M1D F3R	5'_Cttgatatcgaattcctgcaacacgaaattgagctcac_3'	*mad1* D
KA87	M2D5F1bfT F	5'_ccaccgcggtggcggccgctatccagctcgatccatcttg_3'	*mad2* D
KA88	M2D5F1bfTR	5'_aatatagtggcatgattgaaagaataaacatcatgtctgcc_3'	*mad2* D
KA89	M2D3F3afT F	5'_gatggctagagtagaacttaacttcttctttaaccgcttg_3'	*mad2* D
KA90	M2D3F3afT R	5'_agggaacaaaagctgggtacggtggatggacaaaatgaag_3'	*mad2* D
KA111	M1 5 1100	5'_TGGGACGTACGATACGAGCGTTGAGAATTG_3'	*mad1* D screen
KA112	M1 3 1100	5'_TTTCACAGGTAACGCTCATCCCTGCAAAAA_3'	*mad1* D screen
KA153	Cse4mCF	5'_TGGAGCTCCACCGCGGTGGCTCATGGAGAAGA TAGATTGTATAG _3'	Cse4 tagging
KA154	Cse4mCR	5'_GGATCCACTAGTTCTAGAGCGCTCAAATCGTAA TCCTTC _3'	Cse4 tagging
KA155	M1CT F	5'_TACTTCCAATCCAATGCAGATGCCGTAGGCGAA ATGAGC _3'	LIC Cloning
KA157	M1CTiiR	5'_TTATCCACTTCCAATGTTATTATCATCCAAGCCC GACATACCCAG_3'	LIC Cloning
KA160	HG F	5'_TGGAGCTCCACCGCGGTGGCGGTACCGAGCTC GGCAGATAC _3'	GFP-Mad1 tagging
KA161	HG R	5'_TTATTGGCATCATCTCTTCCGTGTTAATACAGAT AAACCAAG_3'	GFP-Mad1 tagging
KA162	HGM1 F	5'_GGAAGAGATGATGCCAATAACCCCGGCTC_3'	GFP-Mad1 tagging
KA163	HGM1 R	5'_GGATCCACTAGTTCTAGAGCGCAAGTCAGGATA GCAGAGTG_3'	GFP-Mad1 tagging
KA182	TEF Promo F	5'_taccgtatagcatagaatggc_3'	Blaster screen
KA183	Ade6 Term R	5'_ATCATCTACTATATGCTTCGTAAATGTCCA_3'	Blaster screen
KA186	MIM F	5'_Gtgcaggattgttacgaagttcggcgcatgcttcgtaagcggggttga actct_3'	Mutagenesis
KA187	MIM R	5'_Agagttcaaccccgcttacgaagcatgcgccgaacttcgtaacaatc ctgcac_3'	Mutagenesis
KA188	Mad2_5_1100k b F	5'_ACACCGGCAAAGTCACTTTCAGATCCG_3'	*mad2* D screen
KA189	Mad2_3_1100k b R	5'_CTTTCAGTGATCCTGAAGGAATCGAGCA_3'	*mad2* D screen
KA256	T661A_F	5'_Caaacatctccgctgtcacttgtgccaaaaaccct_3'	Mutagenesis
KA257	T661A_R	5'_Agggtttttggcacaagtgacagcggagatgtttg_3'	Mutagenesis
KA262	T67A_F	5'_Aaaaaaaaagaacctactgtagccttctcaaacatctccgttgtc_3'	Mutagenesis
KA263	T67A_R	5'_Gacaacggagatgtttgagaaggctacagtaggttctttttttt_3'	Mutagenesis

KA264	T68A_F	5'_Ggaaaaaaaaagaacctactgcagtcttctcaaacatctccgt_3'	Mutagenesis
KA265	T68A_R	5'_Acggagatgtttgagaagactgcagtaggttctttttttttcc_3'	Mutagenesis
KA320	T667E For	5'_Cagggaaaaaaaaagaacctactgtttccttctcaaacatctccgttg tcact_3'	Mutagenesis
KA321	T667E Rev	5'_Agtgacaacggagatgtttgagaaggaaacagtaggttctttttttttcc ctg_3'	Mutagenesis
KA322	T668E For	5'_Aaaaaaaaagaacctacttcagtcttctcaaacatctccgttgtcactt gt_3'	Mutagenesis
KA323	T668E Rev	5'_Acaagtgacaacggagatgtttgagaagactgaagtaggttctttttttt t_3'	Mutagenesis
IL222	Gal7_Fwd	5'_cggccgctctagaactagtgaagatatatatagtaataaatttgaaatg aac_3'	Gal-myc-Mps1 Expression
IL226	Gal7_rev_myc	5'_attcagatcctcttcagagatgagcttttgctccattctcaggagagaatt gag_3'	Gal-myc-Mps1 Expression
IL227	Mps1_Fw_myc	5'_atggagcaaaagctcatctctgaagaggatctgaatatgagctcacc cgagaac_3'	Gal-myc-Mps1 Expression
IL231	Mps1_rev	5'_cgaattcctgcagcccggggtcctgacatatggaccttg_3'	Gal-myc-Mps1 Expression
TD32	Mps1_481_LIC_ Fw	TACTTCCAATCCAATGCAACTTTATTTCATGTGAAC GGA	Kinase domain
TD34	Mps1K_845_LI C_Rv	TTATCCACTTCCAATGTTATTATCTAGACAATGCGT TTTGAGC	Kinase domain

Cryptococcus neoformans transformation protocol

Strains were pre-cultured in YPDA, then diluted overnight into 100ml of culture. These cultures were grown at 30ºC (25 ºC for *bub1Δ*) until the OD_{600} reached 0.3-0.36 the next morning. Cells were harvested, washed twice with 50ml iced cold water and once with 50ml of ice-cold electroporation buffer [10mM Tris-HCl pH7.5, 1mM $MgCl_2$ and 270mM sucrose]. Then cells were resuspended in 35ml electroporation buffer containing 150µl of 1M DTT and incubated for 15 mins on ice. Cells were then spun, washed with 50ml electroporation buffer, and finally resuspended in ~100µl of electroporation buffer. 40µl of cell suspension was gently mixed with linearised DNA (~4µg) and transferred to pre-cooled electroporation cuvettes (2mm). Electroporation was performed at 1400V, 600ohm and 25µF (Biorad, GenePulser). Following electro-pulse cells were incubated on ice for two minutes then 1 ml pre-warmed (30 ºC) YPDA was added to the cells before plating on YPDA. After overnight recovery, cells were replica-plated to selection plates. Colonies were typically tested by PCR for correct integration and then by western blot for protein expression.

Knockout constructs

Both *mad1* and *mad2* knockout constructs were made using the Blaster construct [16]. 1 kb homologous arms, consisting of the *MAD* 5' and 3' UTR sequences, were ligated at

either end of the selective amds2 marker: BlueScript vector was digested with HindIII/EcoRI, and pPEE8 with SpeI/HindIII. The final construct for *mad1Δ* was digested with KpnI and AatII. For *mad2Δ,* SapI and SacII were used to digest the construct before transformation into the wild type H99 strain. Transformed colonies were initially selected on acetamide plates. Cell were re-streaked several times to ensure stable integration and then streaked to single colonies to ensure that all cells contained the Blaster construct. Correct integration of the marker for *mad1Δ* was confirmed by PCR (SFig.1) and by immunoblotting using the *Cryptococcus* anti-Mad1 antibody (Fig.1C). In a similar way, to confirm the *mad2Δ,* PCR analysis was performed with genomic DNA made from stable transformants (Fig.2B).

Mad1 antibody generation and affinity purification

Residues 1-200 of Mad1 were amplified from cDNA and cloned into a LIC Biobrick vector (14C, 6xHis-MBP, https://www.addgene.org/48284/). This Mad1 construct was expressed in *E. coli* pLysS cells (Agilent), purified on Talon Cobalt resin, eluted and then dialysed into 50mM Hepes pH7.6, 75mM KCl. The recombinant protein was used to immunise sheep (MRC PPU Reagents and Services, University of Dundee). Specific antibodies were affinity-purified using Affigel 10 resin coupled to the 6xHis-MBP-Mad1 protein. Sheep sera was diluted with PBS, filtered, then gently pumped through the Affigel-Mad1 column overnight. The column was thoroughly washed with PBS-Tween and then with PBS containing 0.5M NaCl. Finally, the specific anti-Mad1 antibodies were eluted at high pH, with 100 mM triethylamine (pH 11.5), and quickly neutralised before dialysing the antibodies overnight into PBS containing 40% glycerol.

HISp-GFP-MAD1

For Gibson assembly of HISp-GFP-MAD1 the pCN19 vector was used to amplify GFP containing an intron. The HIS promoter and full length *MAD1* clone were PCR-amplified from H99 genomic DNA. The resulting three amplified fragments were Gibson assembled into the pPEE37 safe haven vector (developed by James Fraser). Plasmids were sequenced and the final construct digested with PacI enzyme to target homologous recombination to the correct chromosomal safe-haven locus.

Mad1 alleles (T661A, T667A, T668A, TT667,668AA and RLK-AAA)

The HISp-GFP-Mad1 plasmid was mutagenized using the Quickchange lightning kit (Agilent), according to the manufacturer's instructions.

GALp-myc-MAD2

MAD2 was ectopically expressed to rescue the *mad2Δ* phenotype. Ectopic expression of myc-tagged Mad2 was generated under the P_{GAL7} promoter. The *GAL7* promoter, myc tag (EQKLISEEDLN) and *MAD2* ORF with its 3'UTR were assembled into pPEE37 (HYG resistance, chromosome 3 safe-haven) using Gibson assembly.

MAD2p-MAD2

For a later experiment (Fig.4B) a genomic *MAD2* clone, with its own promoter, was used to rescue the *mad2Δ.*

Cse4-mCherry

Cse4 was tagged with mCherry at the N-terminus and ectopically expressed for use as a centromere marker. This construct was generated under the endogenous Cse4 (1kb) promoter. The promoter and full length *CSE4* clone were PCR-amplified from H99 genomic DNA. These two fragments along with amplified mCherry were cloned into vector pPEE31 (NAT resistance, chromosome 14, safe-haven 7 near CNAG 05557, pEE31) using Gibson assembly.

lacO array

A 240xlacO array was released from pLAU43 [28] as an Nhe1-Xba1 fragment, and then blunt end ligated into the pPEE37 vector. After linearisation this DNA was transformed into the wild-type H99 strain, to integrate at the safe-haven on chromosome 3.

HISp-mNeonGreen-lacI

A *Cryptococcus*-optimised mNeonGreen ORF, containing an intron to boost expression, was synthesised. Codon usage for mNeonGreen was randomly generated from the codon frequency table for the most translated 5% of CDS in H99 (cite PMID: 32020195). Intron 1 from CNAG_05249, with a modified 5' (GTATGT) and 3' (CAG) splice site designed by Huang et al. (cite PMID: 34791226), was inserted into mNeongreen after Lys50. This was then combined with the HIS promoter, lacI ORF and pPEE36 vector (G418 resistance, chromosome 14, targeting safe-haven 7 next to CNAG_05557), through Gibson assembly.

GALp-Myc-MPS1

Mps1 was over-expressed ectopically using a *GALp-myc-MPS1* construct. Endogenous *MPS1* and Gal7 promoter were PCR-amplified from H99 genomic DNA. All three fragments were cloned into vector pPEE36 (G418 resistance, chromosome 14, targeting safe-haven 7 next to CNAG_05557) using Gibson assembly.

Microscopy

Live-cell microscopy was performed with a spinning disc confocal microscope (Nikon Ti2 CSU-W1) with a 100X oil objective (Plan Apo VC) coupled to a Teledyne-Photometrics 95B sCMOS camera. For imaging, Z-stacks of 11 images (step size 0.5µm) were acquired using a 491nm laser line for GFP and 561nm laser for mCherry. Exposure times were typically 300ms and laser power was kept to the minimum to avoid photobleaching. Images were captured using Nikon Elements software.
ImageJ was used for image analysis, which were then further processed in Adobe Photoshop to adjust brightness and contrast. All adjustments were applied to whole images uniformly, and to all images being compared.

Checkpoint assays

Benomyl plates - *serial dilution assay*

Cells from an overnight culture were diluted to OD_{600} ~0.4 in distilled water. Then 10-fold, serial dilutions were made and spotted onto YPDA plates (with or without the anti-microtubule drug, benomyl at different concentrations) then typically incubated at $30^{O}C$ for 48 hours.
Benomyl stock was 30mg/ml in DMSO and, due to solubility issues, this was added directly to boiling YPD agar.

Re-budding assays

Glycerol stocks of *Cryptococcus* strains were stored at -80ºC. Cells were streaked out on YPDA plates and allowed to grow on plates for two days at 30ºC. After two days, cells were grown overnight (to OD_{600} of ~0.5) in 500mls of YPDA media. For mitotic arrest, 2.5µg/ml nocodazole was added to the cells and incubated for three hours. Cells were harvested by centrifugation at 5000 rpm at room temperature, for 3 mins. Following this, cells were washed with distilled water twice and mounted on slides for microscopy. Careful microscopic observation has been made to determine percentage of mitotic arrested cells

with large buds. Cells with bud size greater than 4μm has been categorized as 'Large budded' mitotic arrested cells. While cells having daughters size ranging from 0.5-4μm were categorized as 'small budded'. From microscopic images of fixed cells, the percentage of large-budded cells were calculated and compared between wild type and knockout strains. This experiment was repeated three times with similar results. 300 cells were counted per strain, in each experiment. GraphPad prism version 8 was used for statistical analyses.

Re-budding assay in microfluidics

We used Alcatras microfluidic cell traps incorporated into a device allowing for use with five strains [54]. We moulded devices in polydimethylsiloxane (PDMS) from an SU8-patterned wafer with an increased thickness of 7μm, to accommodate the larger size of *C neoformans* cells compared to *S cerevisiae* (manufactured by Micro-resist, Berlin, design available on request). Imaging chambers for individual strains are isolated by arrays of PDMS pillars separated by 2μm gaps. This prevents intermixing of strains while cells experience identical media conditions.

Before use we filled the devices with synthetic complete (SC) media, supplemented with 0.2g/l glucose and containing 0.05%w/v bovine serum albumin (Sigma) to reduce cell-cell and cell-PDMS adhesion. Cells pre-grown to logarithmic phase in the same media (lacking the BSA) were injected into the device. An EZ flow system (Fluigent) delivered media at 10μl per minute to the flow chambers and performed the switch to media containing nocodazole after 5 hours. This media also contained Cy5 dye to allow monitoring of the timing of the media switch. We captured image stacks at 5-minutes intervals at 4 stage positions for each strain, using a Nikon TiE epifluorescence microscope with a 60x oil-immersion objective (NA 1.4), a Prime95b sCMOS camera (Teledyne Photometrics) and OptoLED illumination (Cairn Research). Image stacks had 5 Z-sections, separated by 0.6μm, captured using a piezo lens positioning motor (Pi).

Sister-chromatid separation assay

We observed the dynamics of chromosome three of *Cryptococcus* strains in living cells using *lacO*-mNeonGreen-lacI system. This system has been adapted for use in *Cryptococcus neoformans* by expressing mNeonGreen-lacI under the Gpd1 promoter. We targeted integration of the *lacO* array in chromosome three at safe-haven 3 near

CNAG_02589. Cells were grown to OD_{600} of ~0.4 in 500mls of YPDA. For mitotic arrest, 2.5µg/ml nocodazole was added to the cells and incubated for three hours. Cells were harvested by centrifugation at 5000 rpm at room temperature, for 3 mins. Following this, cells were washed with distilled water twice and mounted on slides for microscopy. Careful microscopic observation determined if separation of two mNeonGreen-lacI dots representing the replicated sister chromatids had occurred or not.

Mps1 overexpression assays

Cryptococcus strains were grown overnight (to OD_{600} of ~0.5) in 500mls of YP media. Next morning, 2% galactose was added to the cultures and incubated for a further three hours. Cells were then harvested by centrifugation at 5000 rpm at room temperature, for 3 mins. Following this, cells were washed with distilled water twice and mounted on slides for microscopy. From microscopic images, metaphase arrested cells with short mitotic spindles were counted and analysed using GraphPad prism version 8.

Immunoblot analysis

For whole-cell lysates, typically a 10 ml (OD_{600} ~0.5) cell culture was harvested by centrifigation. Cells were washed once and snap frozen in liquid nitrogen. Frozen pellets were resuspended in 2x sample buffer with 200mM DTT and 1mM PMSF. Cells were then disrupted with 0.5mm Zirconia/Silica beads (Thistle Scientific) using a multi-bead beater for 1 min (BioSpec Products). Samples were spun, boiled for 5 min at 95^{o}C, and the cell debris pelleted by centrifugation for 5 min at 13000 rpm. Cleared extracts were then immediately loaded and separated by SDS-PAGE. Proteins were transferred onto nitrocellulose membrane (Amersham Protran 0.2 µm nitrocellulose, GE Healthcare Lifescience) using a semi-dry transfer unit (TE77, Hoefer, Inc, MA, USA) in 25mM Tris, 130 mM glycine and 20% methanol. Transfer was typically for 1.5-2 hours at 150-220 mA. Efficiency of protein transfer was visualised using Ponceau S solution. Membranes were blocked with Blotto (PBS, 0.04% Tween 20, 4% Marvel skimmed milk powder) for at least 30 min at room temperature on a shaking platform. The primary antibody (anti-Bub1, anti-GFP or anti-HA) was incubated in the same blocking buffer (1 in 1000 dilution) overnight at 4^{o}C. The membrane was then washed 3 times for 10 mins with PBS+0.04% Tween and then incubated with the secondary antibody (1 in 5000 dilution) for at least an hour at room temperature. The membrane was washed again, rinsed with PBS and ECL performed

(SuperSignal West Pico, or SuperSignal West Femto, Thermo Fisher Scientific Inc, IL, USA).

Mps1 purifications and kinase assays

Residues 478-784 of CnMps1 were amplified from cDNA and cloned into the 14S Biobrick vector. Induction of protein expression was performed in BL21 (pLysS) cells. IPTG was added and cultures incubated for 16 hrs at 18^{o}C. Cells were harvested, washed and pellets frozen in liquid nitrogen. Cell pellets were resuspended in lysis buffer [50mM Tris-HCl pH8, 500mM NaCl, 10% glycerol, 5mM imidazole, 1mM β-mercaptoethanol, EDTA-free protease inhibitor tablet (Roche), 1mM PMSF] then lysed by sonication (1 sec ON and 2sec OFF for a total of 3 min). To remove the cell debris, lysed cells were centrifuged at 20,000 rpm, for 30-45 min, at 4°C, and the lysate filtered through a 0.45μm syringe. Lysates were then incubated with rotation for 2 hours (at 4°C) with Talon cobalt resin (Thermofisher). After incubation, the beads were transferred to a Biorad column, washed with 10 column volumes of wash buffer, and protein eluted with lysis buffer containing 250mM imidazole. The recombinant kinase domain was dialysed overnight into 50mM Tris-HCl pH8, 150mM NaCl, 5% glycerol, 2mM DTT and proteins concentrated via centrifugation (Vivaspin, Sartorius). Recombinant kinase was added to 10µl of 2X kinase buffer [40mM Hepes (pH 7.5), 200mM KCl, 20mM $MgCl_2$, 2mM DTT, 400µM ATP], substrate, and water to a final volume of 20µl. Reactions were incubated at 30°C for 30 min and quenched with an equal volume of SDS-PAGE sample buffer and run on an SDS-PAGE gel. Immunoblot analysis was performed as above, with anti-His and anti-T120 phosphoantibody (Active motif, 39391).

Radioactive Mps1 kinase assays were performed in a similar reaction for 30 min at 30°C: 20mM Hepes (pH 7.5), 100mM KCl, 10mM $MgCl_2$, 1mM DTT, 100µM cold ATP, 5μCi γ-^{32}P-labelled-ATP and 1 μg substrate.

Lysis of large-scale cell extracts for mass spectrometry

Yeast cells were grown overnight (to OD_{600} of ~0.5) in 500mls of YPDA. 2.5µg/ml nocodazole was added to the cells and incubated for three hours. Cells were harvested by centrifugation at 5000 rpm at 4^{o}C, for 15 mins. Pelleted cells were frozen in drops, using liquid nitrogen. The cells were then ground manually, using a ball grinder. Yeast powders

were resuspended into lysis buffer containing 50mM Hepes pH7.6, 75mM KCl, 1mM MgCl2, 1mM EGTA, 10% Glycerol, 0.1% Triton X-100, 1mM Na_3VO_4, 10 µg/mL CLAAPE (protease inhibitor mix containing chymostatin, leupeptin, aprotinin, antipain, pepstatin, E-64 all dissolved in DMSO at a final concentration of 10 mg/mL), 1 mM PMSF, 0.01 mM microcystin. 1g of yeast powder was resuspended in 1ml of the lysis buffer. Cell lysis was completed by sonication (cycles of 5 sec ON, 5 sec OFF for 1 min). After sonication, the cell debris was pelleted (30 min, at 22000 rpm, at 4^{o}C) and the supernatant incubated with anti-GFP TRAP magnetic agarose beads (ChromoTek) for 1 hr at 4^{o}C. The beads were washed at least 9 times with wash buffer (50mM Hepes pH7.6, 75 mM KCl, 1 mM MgCl2, 1 mM EGTA, 10% Glycerol) and once with PBS+0.001% Tween 20. Proteins were eluted from the beads by adding 2X sample buffer containing 200mM DTT and boiled at 95^{o}C for 5-10 min, before running on an SDS-PAGE gel.

GFP-Mad1 mass-spectrometry and volcano plots

Protein samples from all biological replicates were processed at the same time and using the same digestion protocol without any deviations. They were subjected for MS analysis under the same conditions, and protein and peptide lists were generated using the same software and the same parameters. Specifically, proteins were separated on gel (NuPAGE Novex 4-12% Bis-Tris gel, Life Technologies, UK), in NuPAGE buffer (MES) and visualised using InstantBlueTM stain (AbCam, UK). The stained gel bands were excised and de-stained with 50mM ammonium bicarbonate (Sigma Aldrich, UK) and 100% (v/v) acetonitrile (Sigma Aldrich, UK) and proteins were digested with trypsin, as previously described 69. In brief, proteins were reduced in 10mM dithiothreitol (Sigma Aldrich, UK) for 30mins at 37ÅãC and alkylated in 55mM iodoacetamide (Sigma Aldrich, UK) for 20 min at ambient temperature in the dark. They were then digested overnight at 37ÅãC with 12.5 ng trypsin per µL (Pierce, UK). Following digestion, samples were diluted with an equal volume of 0.1% TFA and spun onto StageTips as described previously 70. Peptides were eluted in 40 µL of 80% acetonitrile in 0.1% TFA and concentrated down to 1 µL by vacuum centrifugation (Concentrator 5301, Eppendorf, UK). The peptide sample was then prepared for LC-MS/MS analysis by diluting it to 5 µL with 0.1% TFA.

LC-MS analyses were performed on an Orbitrap Fusion™ Lumos™ Tribrid™ Mass Spectrometer (Thermo Fisher Scientific, UK) coupled on-line, to an Ultimate 3000 HPLC

(Dionex, Thermo Fisher Scientific, UK). Peptides were separated on a 50 cm (2 µm particle size) EASY-Spray column (Thermo Scientific, UK), which was assembled on an EASYSpray source (Thermo Scientific, UK) and operated constantly at 50oC. Mobile phase A consisted of 0.1% formic acid in LC-MS grade water and mobile phase B consisted of 80% acetonitrile and 0.1% formic acid. Peptides were loaded onto the column at a flow rate of 0.3 µL min-1 and eluted at a flow rate of 0.25 µL min-1 according to the following gradient: 2 to 40% mobile phase B in 150 min and then to 95% in 11 min. Mobile phase B was retained at 95% for 5 min and returned to 2% a minute after until the end of the run (190 min). Survey scans were recorded at 120,000 resolution (scan range 350-1500 m/z) with an ion target of 4.0e5, and injection time of 50ms. MS2 was performed in the ion trap at a rapid scan mode, with ion target of 2.0E4 and HCD fragmentation (Olsen et al, 2007) with normalized collision energy of 28. The isolation window in the quadrupole was 1.4 Thomson. Only ions with charge between 2 and 6 were selected for MS2. Dynamic exclusion was set at 60 s.

The MaxQuant software platform 71 version 1.6.1.0 was used to process the raw files and search was conducted against our in-house Cryptococcus neoformans var. grubii protein 25 database, using the Andromeda search engine 72. For the first search, peptide tolerance was set to 20 ppm while for the main search peptide tolerance was set to 4.5 pm. Isotope mass tolerance was 2 ppm and maximum charge to 7. Digestion mode was set to specific with trypsin allowing maximum of two missed cleavages. Carbamidomethylation of cysteine was set as fixed modification. Oxidation of methionine, and phosphorylation of serine, threonine and tyrosine were set as variable modifications. Label-free quantitation analysis was performed by employing the MaxLFQ algorithm 73. Peptide and protein identifications were filtered to 1% FDR. Statistical analysis was performed by Perseus software 74, version 1.6.2.1.

MS Data availability (links to PRIDE will be added here)

Titan cell production and viability analysis

To produce titan cells *in vitro*, yeast were grown overnight in Yeast Nitrogen Base (YNB) with 2% glucose, diluted to OD_{600} 0.001, then transferred to 10%FCS in PBS at 5%CO_2 and 37^{o}C for 3 days [43].

Cells were then spun down, washed twice and resuspended in YPD, then plated on one side of a YPD dissection plate. A Singer MSM needle (50μm diameter tip) was then used to pick up individual titan cells and they were placed at positions on the MSM grid. Plates were then incubated at room temperature (25ºC) for 3 days. Colonies were counted and the plates re-examined under the dissecting microscope for unbudded cells (just the original titan), budded cells and micro-colonies (scored when less than 20 cells).

Figure 1

CnMad1 is conserved and *mad1* mutants are sensitive to anti-microtubule drugs

A) Schematic diagram indicating conserved domains in CnMad1: a Mad2 interaction motif (MIM), putative Bub1 binding motifs (RLK) and the structurally conserved C-terminal domain (RWD fold).

B) Strategy for generating the *mad1Δ* via recombination with the recyclable *amds2* blaster cassette.

C) Anti-Mad1 immunoblot confirms the *mad1* deletion stain. The three strains indicated were grown to log phase, harvested and whole cell extracts generated. The upper 116kD band recognised by the anti-Mad1 antibody is a cross-reacting band, useful here as a loading control.

D) The *mad1Δ* strain is benomyl sensitive and this can be rescued with an ectopic GFP-Mad1 construct. Strains were grown on YPD plates containing the indicated concentrations of benomyl for 3 days at 30ºC.

Figure 2

CnMad2 is conserved and *mad2* mutants are sensitive to anti-microtubule drugs

A) Strategy for generating the *mad2Δ* using the recyclable *amds2* blaster cassette.

B) Confirmation of the *mad2Δ* strain by PCR.

C) Benomyl sensitivity of the *mad2Δ* and complementation with ectopic *GAL-MAD2*. Strains were grown on YPD plates containing the indicated concentrations of benomyl for 3 days at 30ºC.

D) The *mad1,mad2* double mutant does not display a synthetic phenotype. *mad1, mad2, mad1,mad2 double* and *mps1* strains were diluted, plated and grown on YPD plates at the indicated temperatures and drug concentrations for 3 days.

E) Plate reader experiments confirm that *mad1, mad2* and *mps1* mutants are all temperature sensitive. Cells were diluted to OD_{600} 0.2 and grown with shaking at the indicated temperatures.

Figure 3

Cn*mad1*Δ and *mad2*Δ strains fail to checkpoint arrest

A) *mad1*, *mad2* and *mps1* strains fail to maintain a large-budded arrest. The strains indicated were grown to log phase and then nocodazole was added to a final concentration of 2.5 μg/ml in YPD media for the final 3 hours. Scale bar is 10μm.

B) Quantitation of the large-budded cells observed at the 3 hour time point during this nocodazole challenge. This experiment was repeated 3 times and 300 cells were counted for each strain per experiment.

C) Images taken from a microfluidics analysis of this behaviour in nocodazole (for H99, *mad1, mad2 and mps1* mutants). Cells were pre-grown in synthetic complete media supplemented with 0.2g/ml glucose and 0.05% w/v bovine serum albumin (Sigma) and then injected into the microfluidics device and analysed for X hours (+/- 2.5μg/ml nocodazole). Scale bar is 10μm.

D) Quantitation of the microfluidics experiment: movies were analysed manually for re-budding. This experiment was repeated three times and at least 100 cells counted per strain each time.

Figure 4

The *mad2*Δ mutant fails to maintain sister-chromatid separation

A) Schematic representation of the strain with fluorescently-marked chromosome 3. An array of 240 lac operators were integrated at the safe-haven on chromosome 3 and lacI-mNeonGreen expressed.

B) mNeonGreen was imaged in YPD cultures of 'wild-type' (*mad2*Δ, complemented by an ectopic *MAD2* construct) and *mad2*Δ strains, 3 hours after the addition of 2.5μg/ml nocodazole. Scale bar is 10μm.

C) Quantitation of this experiment after three biological repeats. 100 cells were scored in each condition for each experiment. Note, as nocodazole is present there are no microtubule spindles to pull sister chromatids apart in this experiment, so not all appear to separate.

Figure 5

CnMad1 accumulates at the nuclear periphery during interphase and is then recruited to unattached kinetochores in mitosis

A) Strains expressing GFP-Mad1 were stained with Hoechst to label their DNA in cultures grown with and without the addition of 2.5μg/ml nocodazole. Scale bar is 10μm.
B) Six representative stages of mitosis are shown here, from live imaging of a strain expressing both GFP-Mad1 and mCherry-Tub4 (the gamma tubulin construct labels the spindle poles in mitosis). Scale bar is 10μm.
C) In nocodazole arrested cells, GFP-Mad1 is close to but does not co-localise with spindle poles (mCherry-Tub4). Scale bar is 10μm.
D) In nocodazole arrested cells, GFP-Mad1 does co-localise with the kinetochore marker, mCherry-Dad2. Scale bar is 10μm.
E) In nocodazole arrested cells, GFP-Mad1 does co-localise with the centromere marker Cse4-mCherry. Scale bar is 10μm.

Figure 6

CnMad1 interacts with Mad2, Bub1, Bub3 and several mitotic regulators including Cdc20-APC/C.

GFP-Mad1 was immunoprecipitated from extracts using GFP-TRAP and immunoprecipitates were run into an SDS-PAGE gel, cut out and digested into peptides with trypsin before analysis on a Orbitrap Fusion™ Lumos™ Tribrid™ Mass Spectrometer. Volcano plots show the difference (mean LFQ difference) and confidence ($-\log_{10}$P-value of Perseus statistical test) between the GFP-Mad1 and untagged control pull-downs (n=3 for each).

A) Analysis of mitotic GFP-Mad1 interactors: cycling GFP-Mad1 v. nocodazole-arrested GFP-Mad1.
B) Analysis of GFP-Mad1 interactors: cycling v. GFP-Mad1 tagged.
C) Cycling versus arrested GFP-Mad1. In interphase, several nucleoporins are specifically enriched, including TPR, Nup62 and Nup155.
D) GFP-Mad1 and mCherry-Bub1 co-localise in mitotic cells.
E) Alignment of the Mad-RLK region in *C. neoformans*, *Homo sapiens*, *Schizosaccharomyces pombe* and *Saccharomyces cerevisiae*. Only the sec ond RLK is conserved.
F) Co-immunoprecipitation of Mad1 and Bub1 is RLK-dependent.

Figure 7

Mps1 overexpression is sufficient to generate a mitotic checkpoint arrest

A) P_{GAL7}-*MPS1* was induced for 5 hours with 2% Galactose, or 2% glucose as the un-induced control. Scale bar is 10μm.

B) Quantitation of this mitotic arrest. Short spindles were scored every hour in at least 100 cells per condition at each time point. This experiment was repeated 3 times and displayed here as the mean +/- confidence levels.

C) Immunoblot of Mps1 levels at each hourly time point after Gal induction. Whole cell extracts were prepared by bead-beating, separated by SDS-PAGE and immunoblotted with the 9E10 anti-myc monoclonal antibody.

D) P_{GAL7}-*MPS1* metaphase arrest is Mad1- and Mad2-dependent. Quantitation of the % large-budded cells at the 5 hour time point (experiment repeated 3 times).

E) Immunoblot of Myc-Mps1 levels in wild-type and *mad* mutants.

Figure 8

Mps1 phosphorylates Mad1 for checkpoint arrest

A) *Mps1 in vitro* kinase assays phosphorylate the Mad1 C-terminus.

B) Quantitation of the phosphorylation of the Mad1 C-terminus.

C) Sequence of Mad1C indicating the Mad1 phospho-sites (red) identified by mass-spectrometry. See supplementary data for sequence of all peptides.

D) The *mad1-T667A* mutant, and the double phospho-mutant, is benomyl sensitive. The strains indicated were grown at 30°C for 3 days.

E) Anti-GFP immunoblot of whole cell extracts. The GFP-*mad1* phospho-mutant proteins are stable.

F) The *mad1-T667A* mutant fails to nocodazole arrest. Cultures were grown to log phase and then challenged with nocodazole for 3 hours. Experiment repeated 3 times.

G) The *mad1-T667A* mutant, and the double phospho-mutant, fails to arrest when Mps1 kinase is over-expressed. Log phase cultures were induced with 2% galactose for 5 hours. Experiment repeated 3 times.

Figure 9

***mad* and *mps1* mutant titan cells have reduced viability**

A) *mad* mutants can form titan cells. The strains indicated were all tested for their ability to form titan cells using the *in vitro* titanisation assay developed by Liz Ballou and colleagues. Cells were stained with india ink after 3 days growth at 37ºC, 5%CO_2, 10%FCS/PBS. For comparison, log phase cultures of the same yeast strains grown in YPD were stained with india ink. Scale bars are 10μm.

B) Not all *mad* and *mps1* titans are viable. Individual titan cells were picked up and placed on a grid using a micro-dissection needle (Singer MSM), then grown for 3 days at 25ºC to test their ability to form viable colonies.

C) Quantitative analysis of titan cell progeny. 100 titan cells were analysed per strain in each experiment. This experiment has been repeated at least 4 times for each strain, by 2 researchers.

References

1. WHO fungal priority pathogens list to guide research, development and public health action. https://wwwwhoint/publications/i/item/9789240060241. 2022.
2. Rajasingham R, Govender NP, Jordan A, Loyse A, Shroufi A, Denning DW, et al. The global burden of HIV-associated cryptococcal infection in adults in 2020: a modelling analysis. Lancet Infect Dis. 2022. Epub 20220829. doi: 10.1016/S1473-3099(22)00499-6. PubMed PMID: 36049486.
3. Fisher MC, Alastruey-Izquierdo A, Berman J, Bicanic T, Bignell EM, Bowyer P, et al. Tackling the emerging threat of antifungal resistance to human health. Nat Rev Microbiol. 2022;20(9):557-71. Epub 20220329. doi: 10.1038/s41579-022-00720-1. PubMed PMID: 35352028; PubMed Central PMCID: PMCPMC8962932.
4. Wertheimer NB, Stone N, Berman J. Ploidy dynamics and evolvability in fungi. Philos Trans R Soc Lond B Biol Sci. 2016;371(1709). doi: 10.1098/rstb.2015.0461. PubMed PMID: 28080987; PubMed Central PMCID: PMCPMC5095540.
5. Kozubowski L, Yadav V, Chatterjee G, Sridhar S, Yamaguchi M, Kawamoto S, et al. Ordered kinetochore assembly in the human-pathogenic basidiomycetous yeast Cryptococcus neoformans. Mbio. 2013;4(5):e00614-13. Epub 20131001. doi: 10.1128/mBio.00614-13. PubMed PMID: 24085781; PubMed Central PMCID: PMCPMC3791896.
6. Gerstein AC, Fu MS, Mukaremera L, Li ZM, Ormerod KL, Fraser JA, et al. Polyploid Titan Cells Produce Haploid and Aneuploid Progeny To Promote Stress Adaptation. Mbio. 2015;6(5). doi: ARTN e01340-15
10.1128/mBio.01340-15. PubMed PMID: WOS:000364523100039.
7. Okagaki LH, Nielsen K. Titan Cells Confer Protection from Phagocytosis in Cryptococcus neoformans Infections. Eukaryot Cell. 2012;11(6):820-6. doi: 10.1128/Ec.00121-12. PubMed PMID: WOS:000307190500012.
8. Altamirano S, Li Z, Fu MS, Ding M, Fulton SR, Yoder JM, et al. The Cyclin Cln1 Controls Polyploid Titan Cell Formation following a Stress-Induced G2 Arrest in Cryptococcus. Mbio. 2021;12(5):e0250921. Epub 20211012. doi: 10.1128/mBio.02509-21. PubMed PMID: 34634930; PubMed Central PMCID: PMCPMC8510536.
9. Musacchio A. The Molecular Biology of Spindle Assembly Checkpoint Signaling Dynamics. Curr Biol. 2015;25(20):R1002-18. Epub 2015/10/21. doi: S0960-9822(15)01045-3 [pii] 10.1016/j.cub.2015.08.051. PubMed PMID: 26485365.
10. London N, Biggins S. Signalling dynamics in the spindle checkpoint response. Nat Rev Mol Cell Biol. 2014;15(11):736-48. Epub 2014/10/11. doi: nrm3888 [pii]
10.1038/nrm3888. PubMed PMID: 25303117.
11. Li R, Murray AW. Feedback control of mitosis in budding yeast. Cell. 1991;66:519-31.
12. Hoyt MA, Totis L, Roberts BT. S. cerevisiae genes required for cell cycle arrest in response to loss of microtubule function. Cell. 1991;66:507-17.
13. Weiss E, Winey M. The Saccharomyces cerevisiae spindle pole body duplication gene MPS1 is part of a mitotic checkpoint. Journal of Cell Biology. 1996;132(1-2):111-23.
14. Kops G, Snel B, Tromer EC. Evolutionary Dynamics of the Spindle Assembly Checkpoint in Eukaryotes. Curr Biol. 2020;30(10):R589-R602. doi: 10.1016/j.cub.2020.02.021. PubMed PMID: 32428500.
15. Lee KT, So YS, Yang DH, Jung KW, Choi J, Lee DG, et al. Systematic functional analysis of kinases in the fungal pathogen Cryptococcus neoformans. Nat Commun. 2016;7:12766. doi: 10.1038/ncomms12766. PubMed PMID: 27677328; PubMed Central PMCID: PMCPMC5052723.
16. Erpf PE, Stephenson CJ, Fraser JA. amdS as a dominant recyclable marker in Cryptococcus neoformans. Fungal Genet Biol. 2019;131:103241. Epub 20190617. doi: 10.1016/j.fgb.2019.103241. PubMed PMID: 31220607.

17. Chen RH, Brady DM, Smith D, Murray AW, Hardwick KG. The spindle checkpoint of budding yeast depends on a tight complex between the Mad1 and Mad2 proteins. Mol Biol Cell. 1999;10(8):2607-18. PubMed PMID: 10436016.
18. Chen RH, Shevchenko A, Mann M, Murray AW. Spindle checkpoint protein Xmad1 recruits xmad2 to unattached kinetochores. J Cell Biol. 1998;143:283-95.
19. Campbell MS, Chan GK, Yen TJ. Mitotic checkpoint proteins HsMAD1 and HsMAD2 are associated with nuclear pore complexes in interphase. J Cell Sci. 2001;114(Pt 5):953-63. PubMed PMID: 11181178.
20. Sironi L, Mapelli M, Knapp S, De Antoni A, Jeang KT, Musacchio A. Crystal structure of the tetrameric Mad1-Mad2 core complex: implications of a 'safety belt' binding mechanism for the spindle checkpoint. Embo J. 2002;21(10):2496-506. PubMed PMID: 12006501.
21. Lan W, Cleveland DW. A chemical tool box defines mitotic and interphase roles for Mps1 kinase. J Cell Biol. 2010;190(1):21-4. Epub 2010/07/14. doi: jcb.201006080 [pii] 10.1083/jcb.201006080. PubMed PMID: 20624898; PubMed Central PMCID: PMC2911672.
22. Maure JF, Kitamura E, Tanaka TU. Mps1 kinase promotes sister-kinetochore bi-orientation by a tension-dependent mechanism. Curr Biol. 2007;17(24):2175-82. Epub 2007/12/07. doi: S0960-9822(07)02271-3 [pii] 10.1016/j.cub.2007.11.032. PubMed PMID: 18060784.
23. Sarangapani KK, Koch LB, Nelson CR, Asbury CL, Biggins S. Kinetochore-bound Mps1 regulates kinetochore-microtubule attachments via Ndc80 phosphorylation. J Cell Biol. 2021;220(12). Epub 20211014. doi: 10.1083/jcb.202106130. PubMed PMID: 34647959; PubMed Central PMCID: PMCPMC8641409.
24. Hayward D, Roberts E, Gruneberg U. MPS1 localizes to end-on microtubule-attached kinetochores to promote microtubule release. Curr Biol. 2022. Epub 20221111. doi: 10.1016/j.cub.2022.10.047. PubMed PMID: 36395767.
25. Sridhar S, Hori T, Nakagawa R, Fukagawa T, Sanyal K. Bridgin connects the outer kinetochore to centromeric chromatin. Nat Commun. 2021;12(1):146. Epub 20210108. doi: 10.1038/s41467-020-20161-9. PubMed PMID: 33420015; PubMed Central PMCID: PMCPMC7794384.
26. Robinett CC, Straight A, Li G, Willhelm C, Sudlow G, Murray A, et al. In vivo localization of DNA sequences and visualization of large- scale chromatin organization using lac operator/repressor recognition. Journal Of Cell Biology. 1996;135(6 Pt2):1685-700.
27. Molnar M, Bahler J, Kohli J, Hiraoka Y. Live observation of fission yeast meiosis in recombination-deficient mutants: a study on achiasmate chromosome segregation. J Cell Sci. 2001;114(Pt 15):2843-53. PubMed PMID: 11683417.
28. Lau IF, Filipe SR, Soballe B, Okstad OA, Barre FX, Sherratt DJ. Spatial and temporal organization of replicating Escherichia coli chromosomes. Mol Microbiol. 2003;49(3):731-43. doi: 10.1046/j.1365-2958.2003.03640.x. PubMed PMID: 12864855.
29. Hardwick KG, Murray AW. Mad1p, a phosphoprotein component of the spindle assembly checkpoint in budding yeast. J Cell Biol. 1995;131:709-20.
30. Lee SH, Sterling H, Burlingame A, McCormick F. Tpr directly binds to Mad1 and Mad2 and is important for the Mad1-Mad2-mediated mitotic spindle checkpoint. Genes Dev. 2008;22(21):2926-31. Epub 2008/11/05. doi: 22/21/2926 [pii] 10.1101/gad.1677208. PubMed PMID: 18981471; PubMed Central PMCID: PMC2577792.
31. Rodriguez-Bravo V, Maciejowski J, Corona J, Buch HK, Collin P, Kanemaki MT, et al. Nuclear pores protect genome integrity by assembling a premitotic and Mad1-dependent anaphase inhibitor. Cell. 2014;156(5):1017-31. doi: 10.1016/j.cell.2014.01.010. PubMed PMID: 24581499; PubMed Central PMCID: PMCPMC3947552.
32. Cunha-Silva S, Osswald M, Goemann J, Barbosa J, Santos LM, Resende P, et al. Mps1-mediated release of Mad1 from nuclear pores ensures the fidelity of chromosome segregation. J

Cell Biol. 2020;219(3). doi: 10.1083/jcb.201906039. PubMed PMID: 31913420; PubMed Central PMCID: PMCPMC7054998.
33. Cairo LV, Ptak C, Wozniak RW. Dual personality of Mad1: regulation of nuclear import by a spindle assembly checkpoint protein. Nucleus. 2013;4(5):367-73. Epub 20130927. doi: 10.4161/nucl.26573. PubMed PMID: 24076561; PubMed Central PMCID: PMCPMC3899126.
34. Kim SH, Lin DP, Matsumoto S, Kitazono A, Matsumoto T. Fission yeast Slp1: an effector of the Mad2-dependent spindle checkpoint. Science. 1998;279(5353):1045-7. PubMed PMID: 9461438.
35. Hwang LH, Lau LF, Smith DL, Mistrot CA, Hardwick KG, Hwang ES, et al. Budding yeast Cdc20: A target of the spindle checkpoint. Science. 1998;279(5353):1041-4.
36. Alfieri C, Chang L, Zhang Z, Yang J, Maslen S, Skehel M, et al. Molecular basis of APC/C regulation by the spindle assembly checkpoint. Nature. 2016;536(7617):431-6. Epub 20160810. doi: 10.1038/nature19083. PubMed PMID: 27509861; PubMed Central PMCID: PMCPMC5019344.
37. Brady DM, Hardwick KG. Complex formation between Mad1p, Bub1p and Bub3p is crucial for spindle checkpoint function. Current Biology. 2000;10:675-8.
38. Heinrich S, Sewart K, Windecker H, Langegger M, Schmidt N, Hustedt N, et al. Mad1 contribution to spindle assembly checkpoint signalling goes beyond presenting Mad2 at kinetochores. EMBO Rep. 2014;15(3):291-8. Epub 20140129. doi: 10.1002/embr.201338114. PubMed PMID: 24477934; PubMed Central PMCID: PMCPMC3989695.
39. Fischer ES, Yu CWH, Bellini D, McLaughlin SH, Orr CM, Wagner A, et al. Molecular mechanism of Mad1 kinetochore targeting by phosphorylated Bub1. EMBO Rep. 2021;22(7):e52242. Epub 20210519. doi: 10.15252/embr.202052242. PubMed PMID: 34013668; PubMed Central PMCID: PMCPMC8391104.
40. Hardwick KG, Weiss E, Luca FC, Winey M, Murray AW. Activation of the budding yeast spindle assembly checkpoint without mitotic spindle disruption. Science. 1996;273:953-6.
41. He X, Jones MH, Winey M, Sazer S. Mph1, a member of the Mps1-like family of dual specificity protein kinases, is required for the spindle checkpoint in S. pombe. J Cell Sci. 1998;111 (Pt 12):1635-47. PubMed PMID: 9601094.
42. Fischer ES, Yu CWH, Hevler JF, McLaughlin SH, Maslen SL, Heck AJR, et al. Juxtaposition of Bub1 and Cdc20 on phosphorylated Mad1 during catalytic mitotic checkpoint complex assembly. Nat Commun. 2022;13(1):6381. Epub 20221026. doi: 10.1038/s41467-022-34058-2. PubMed PMID: 36289199; PubMed Central PMCID: PMCPMC9605988.
43. Dambuza IM, Drake T, Chapuis A, Zhou X, Correia J, Taylor-Smith L, et al. The Cryptococcus neoformans Titan cell is an inducible and regulated morphotype underlying pathogenesis. PLoS Pathog. 2018;14(5):e1006978. Epub 20180518. doi: 10.1371/journal.ppat.1006978. PubMed PMID: 29775474; PubMed Central PMCID: PMCPMC5959070.
44. Hommel B, Mukaremera L, Cordero RJB, Coelho C, Desjardins CA, Sturny-Leclere A, et al. Titan cells formation in Cryptococcus neoformans is finely tuned by environmental conditions and modulated by positive and negative genetic regulators. PLoS Pathog. 2018;14(5):e1006982. Epub 20180518. doi: 10.1371/journal.ppat.1006982. PubMed PMID: 29775480; PubMed Central PMCID: PMCPMC5959062.
45. Mukaremera L, Lee KK, Wagener J, Wiesner DL, Gow NAR, Nielsen K. Titan cell production in Cryptococcus neoformans reshapes the cell wall and capsule composition during infection. Cell Surf. 2018;1:15-24. Epub 20180216. doi: 10.1016/j.tcsw.2017.12.001. PubMed PMID: 30123851; PubMed Central PMCID: PMCPMC6095662.
46. Leontiou I. Bub1 kinase acts as a signalling hub for the entire Cryptococcus neoformans spindle assembly checkpoint pathway. https://doiorg/101101/20220921508923. 2023.

47. Schulze VK, Klar U, Kosemund D, Wengner AM, Siemeister G, Stockigt D, et al. Treating Cancer by Spindle Assembly Checkpoint Abrogation: Discovery of Two Clinical Candidates, BAY 1161909 and BAY 1217389, Targeting MPS1 Kinase. J Med Chem. 2020;63(15):8025-42. Epub 20200427. doi: 10.1021/acs.jmedchem.9b02035. PubMed PMID: 32338514.
48. Iouk T, Kerscher O, Scott RJ, Basrai MA, Wozniak RW. The yeast nuclear pore complex functionally interacts with components of the spindle assembly checkpoint. J Cell Biol. 2002;159(5):807-19. PubMed PMID: 12473689.
49. Stucke VM, Sillje HH, Arnaud L, Nigg EA. Human Mps1 kinase is required for the spindle assembly checkpoint but not for centrosome duplication. EMBO J. 2002;21(7):1723-32. Epub 2002/04/03. doi: 10.1093/emboj/21.7.1723. PubMed PMID: 11927556.
50. Storchova Z, Breneman A, Cande J, Dunn J, Burbank K, O'Toole E, et al. Genome-wide genetic analysis of polyploidy in yeast. Nature. 2006;443(7111):541-7. doi: 10.1038/nature05178. PubMed PMID: 17024086.
51. Hanks S, Coleman K, Summersgill B, Messahel B, Williamson D, Pritchard-Jones K, et al. Comparative genomic hybridization and BUB1B mutation analyses in childhood cancers associated with mosaic variegated aneuploidy syndrome. Cancer Lett. 2006;239(2):234-8. PubMed PMID: 16182441.
52. Janbon G, Ormerod KL, Paulet D, Byrnes EJ, 3rd, Yadav V, Chatterjee G, et al. Analysis of the genome and transcriptome of Cryptococcus neoformans var. grubii reveals complex RNA expression and microevolution leading to virulence attenuation. PLoS Genet. 2014;10(4):e1004261. Epub 20140417. doi: 10.1371/journal.pgen.1004261. PubMed PMID: 24743168; PubMed Central PMCID: PMCPMC3990503.
53. Akera T, Goto Y, Sato M, Yamamoto M, Watanabe Y. Mad1 promotes chromosome congression by anchoring a kinesin motor to the kinetochore. Nat Cell Biol. 2015;17(9):1124-33. Epub 2015/08/11. doi: ncb3219 [pii]
10.1038/ncb3219. PubMed PMID: 26258632.
54. Crane MM, Clark IB, Bakker E, Smith S, Swain PS. A microfluidic system for studying ageing and dynamic single-cell responses in budding yeast. PLoS One. 2014;9(6):e100042. Epub 20140620. doi: 10.1371/journal.pone.0100042. PubMed PMID: 24950344; PubMed Central PMCID: PMCPMC4065030.

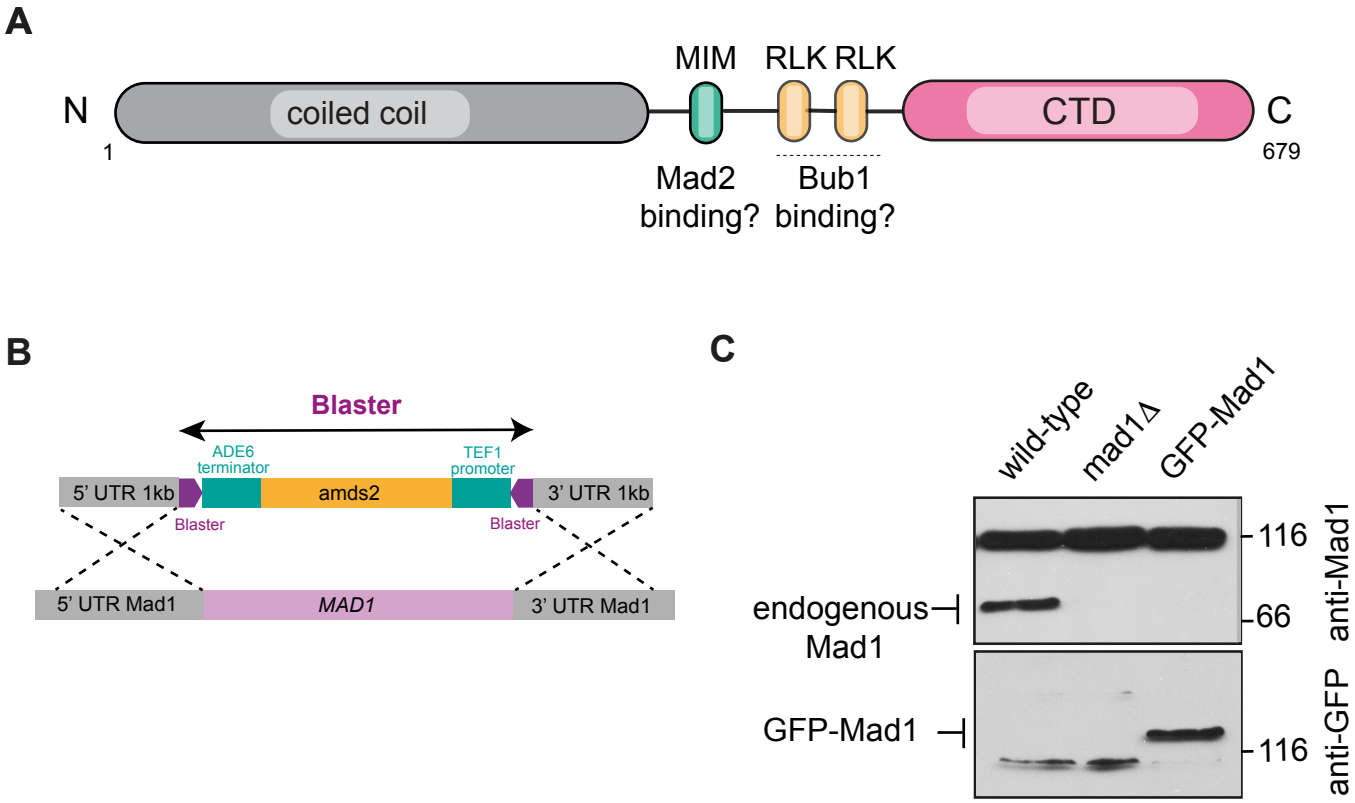

Figure 1 Aktar

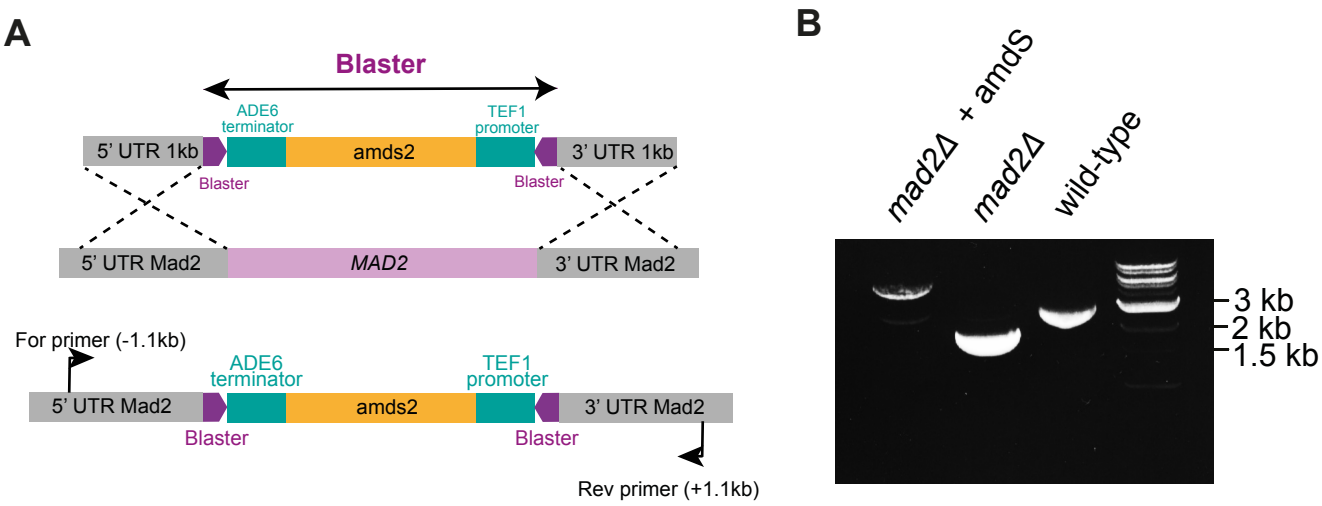

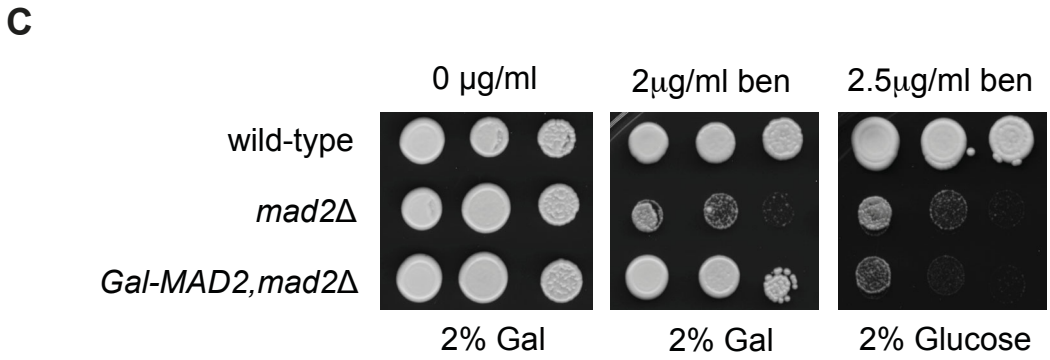

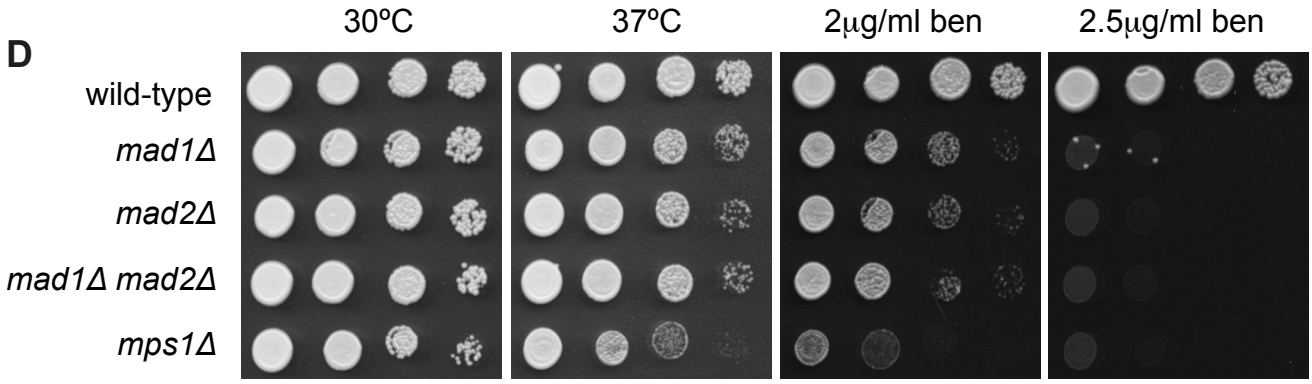

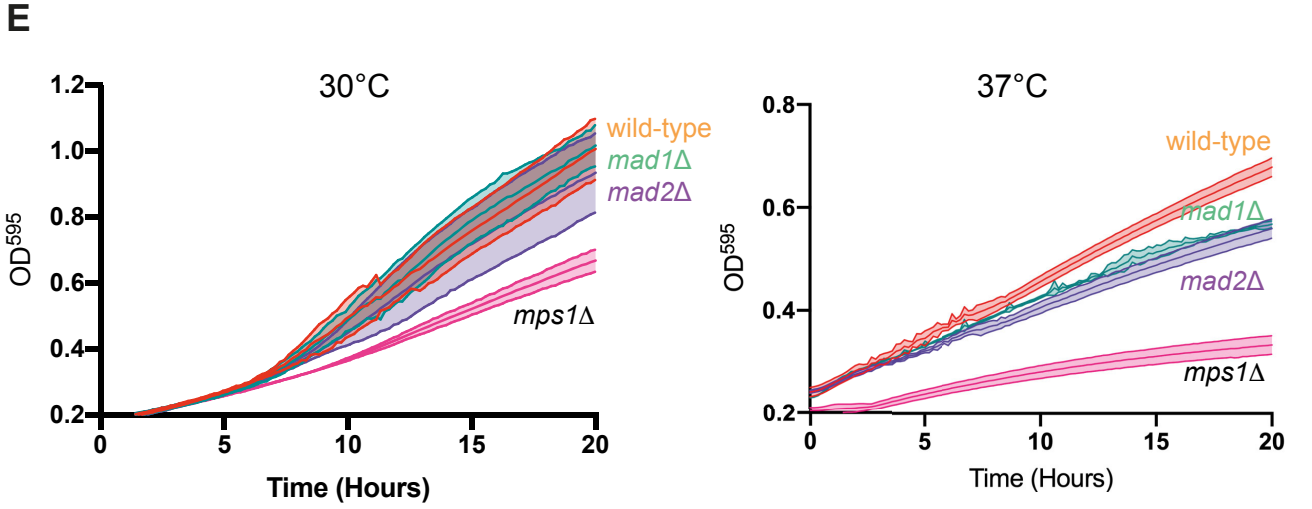

Figure 2 Aktar

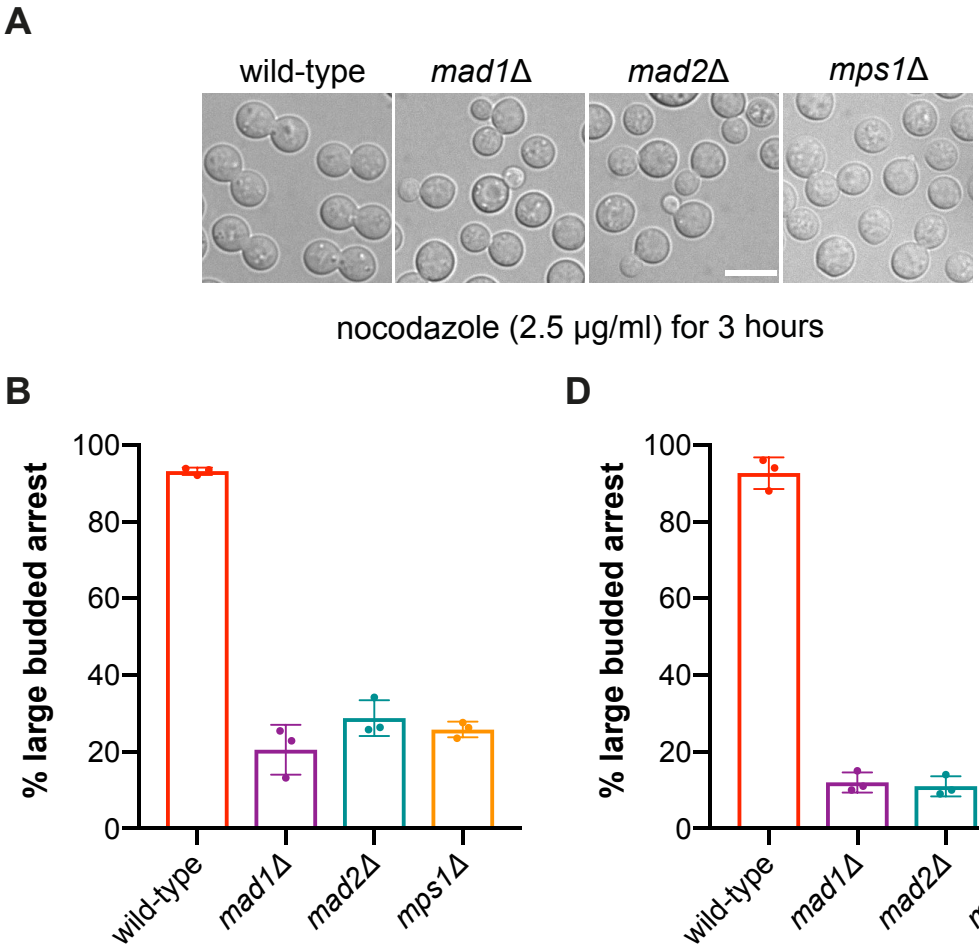

Figure 3 Aktar

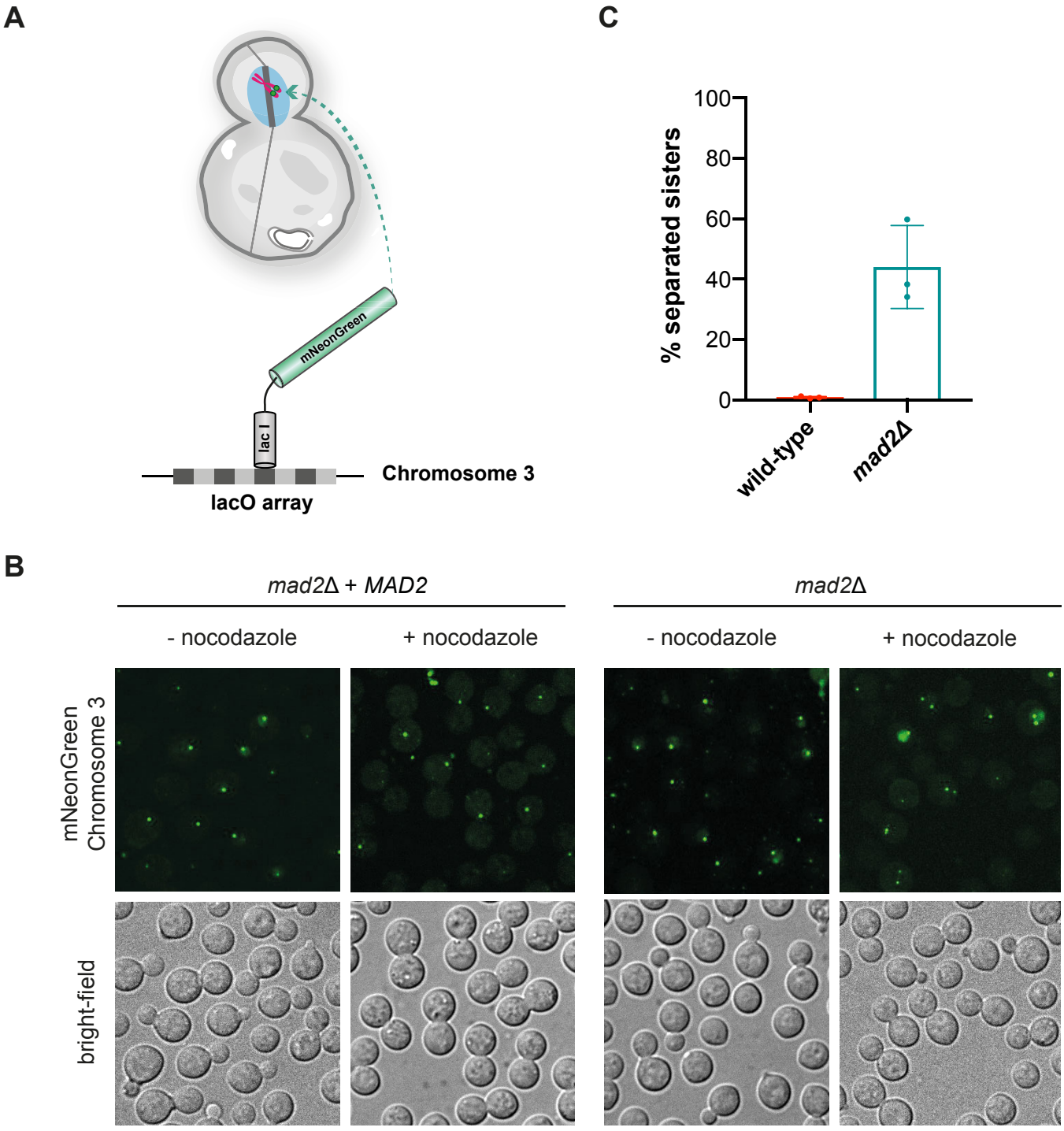

Figure 4 Aktar

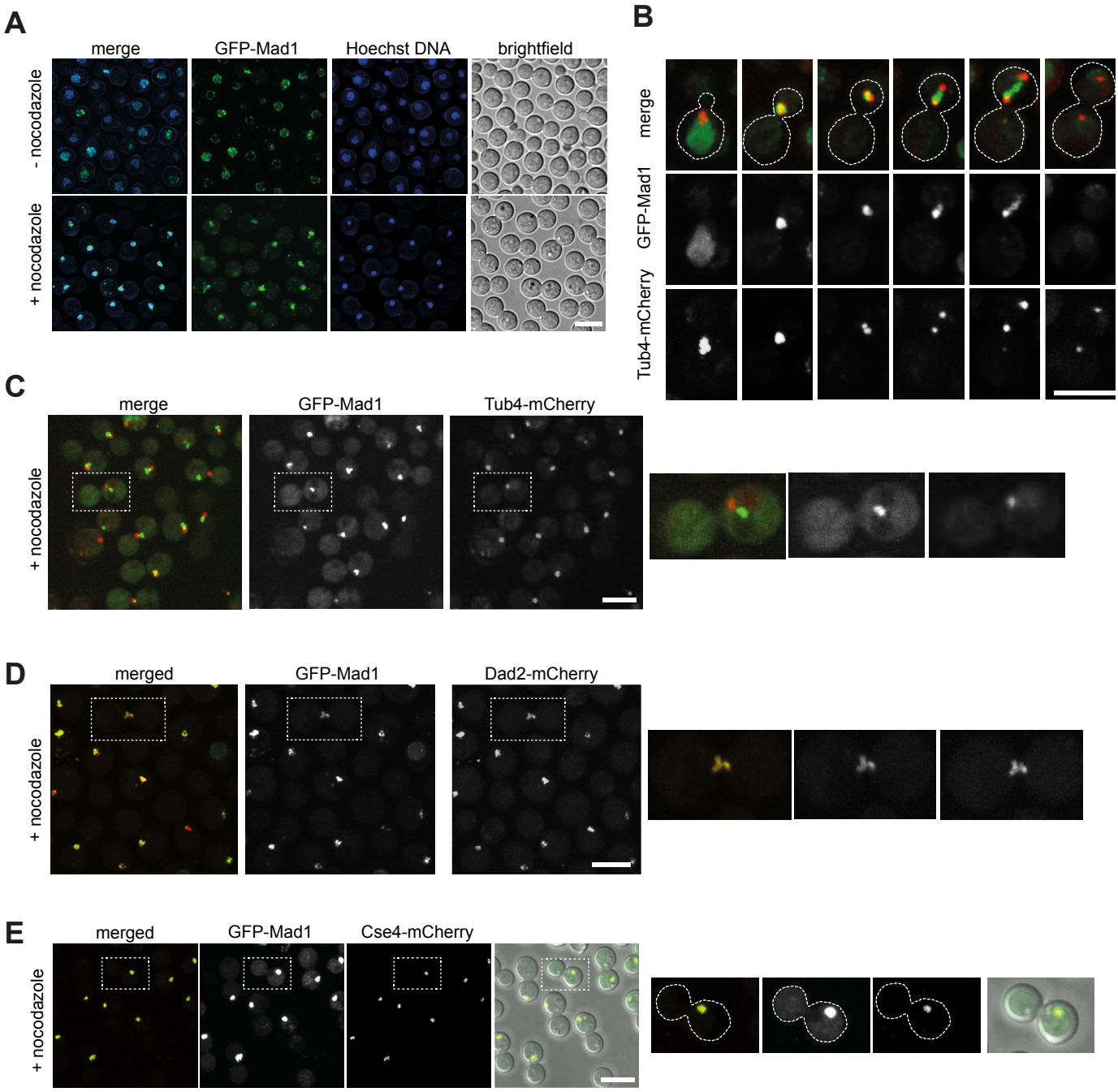

Figure 5 Aktar

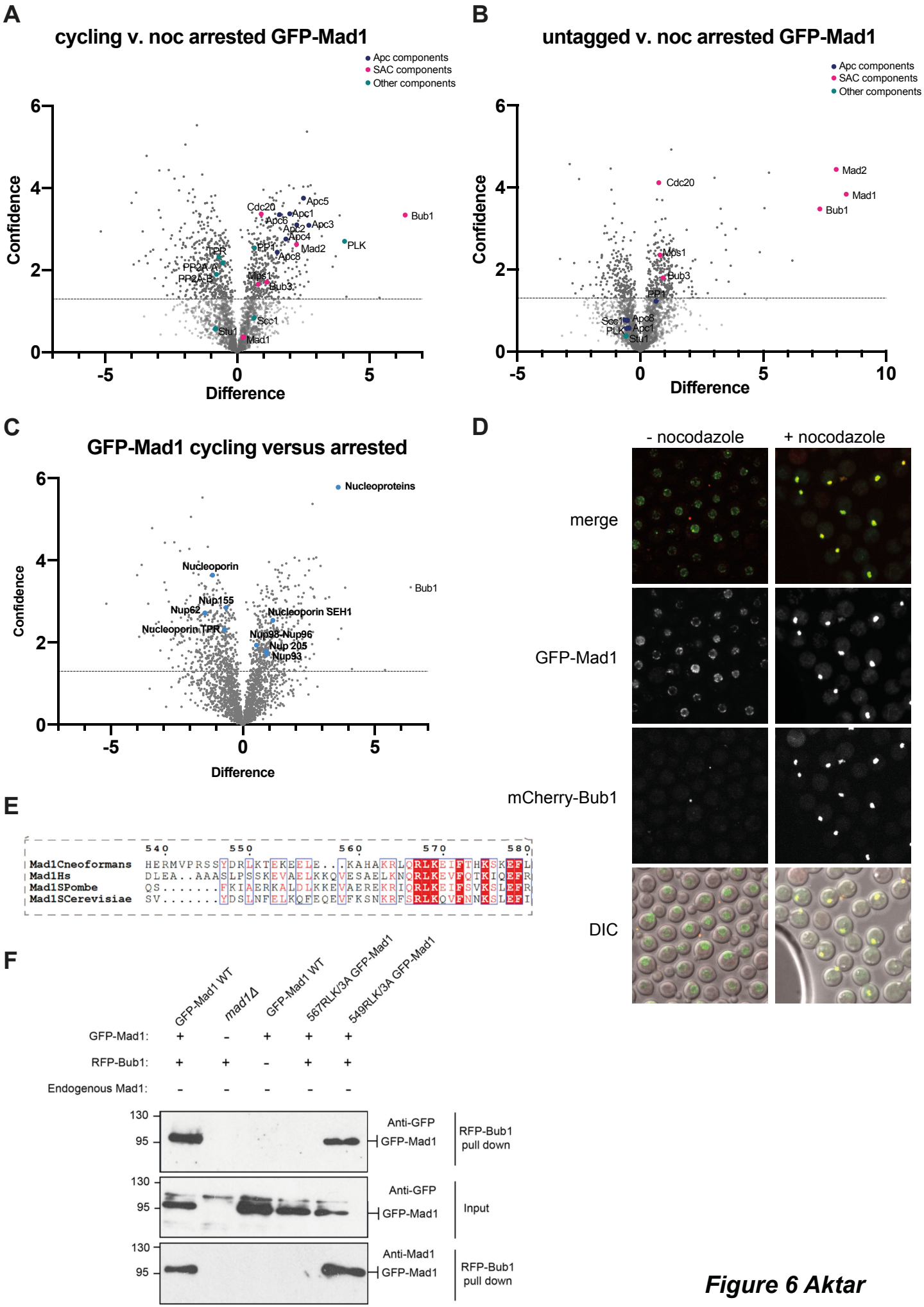

Figure 6 Aktar

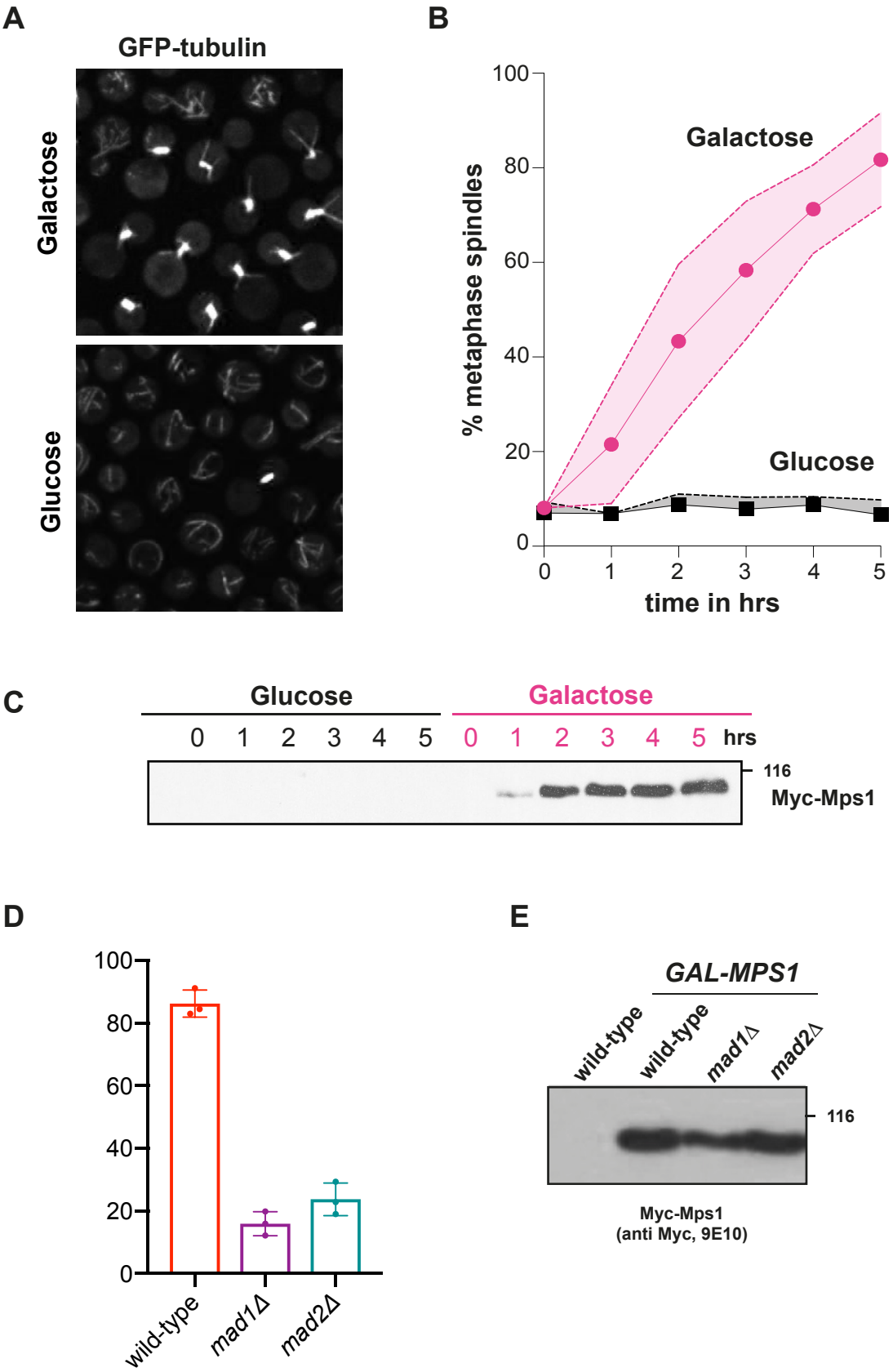

Figure 7 Aktar

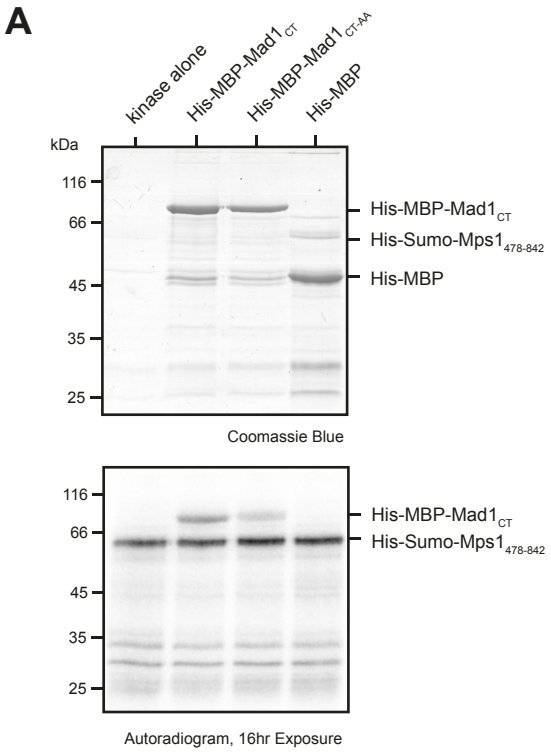

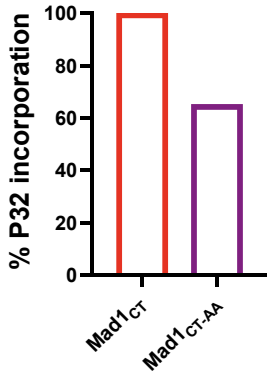

C

Mad1-Cterminus

EMSRRATEAERELRWAKEGRESAERREGLVRKELEAVRRQLAATPGPSAGS
GDPERVKELESLLQSYKTTLEEIHRDSRDAEERIAKGMGLVKSQDLDKAQD
KISQLEEEIAGLSSSVSYLTSSNTALNTEVTNLMQRVASGEFNPAYERCLE
LRNNPAQKIWGIRKQELEDLKAENGELLERLAELDGLLAESQAGVGAGANA
SARGEGVPAHERMVPRSSYDRLKTEKEELEKAHAKRLQRLKEIFTHKSKEF
LEAVYSLLGWRIKFDESGSDIRLTSMYAPKGKNGLTIKFTSSEGHFGTMQM
SGMMARSLEESRQFWVVERQSVPGFLAQVTTEMFEKTTIGRAAGYVGLG*

667/668

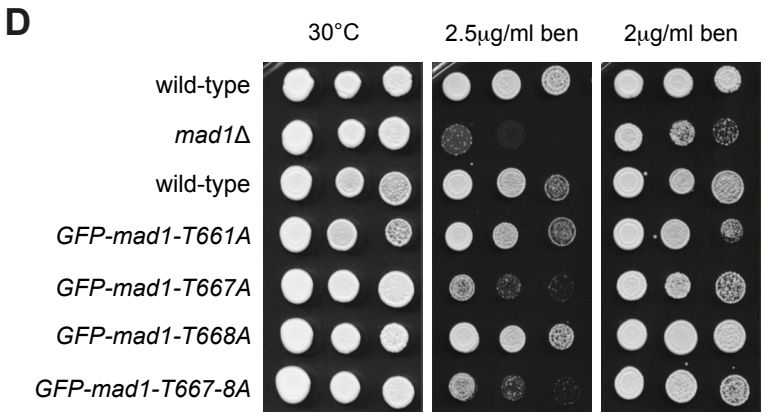

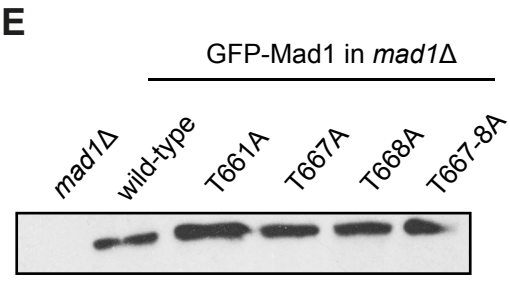

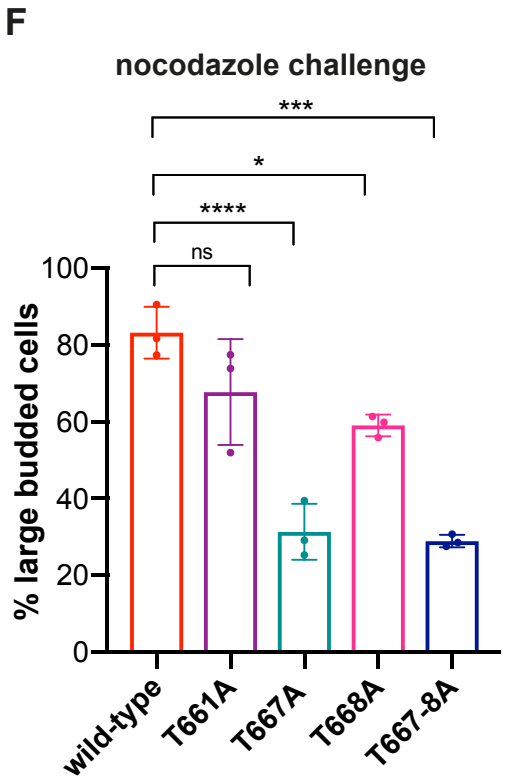

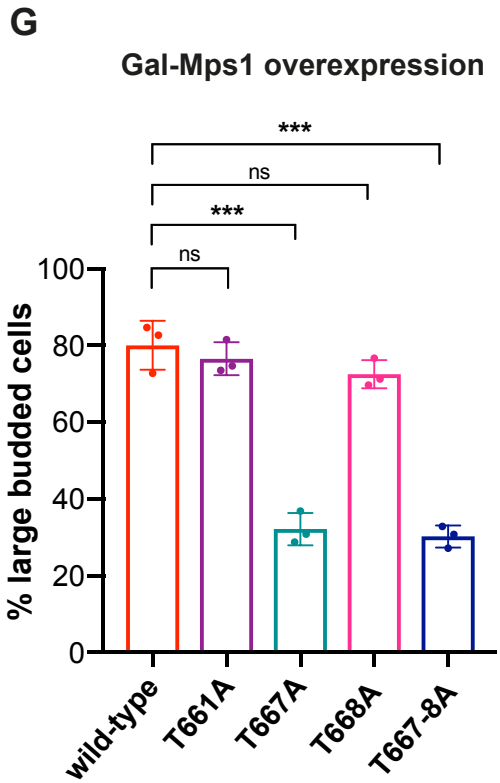

Figure 8 Aktar

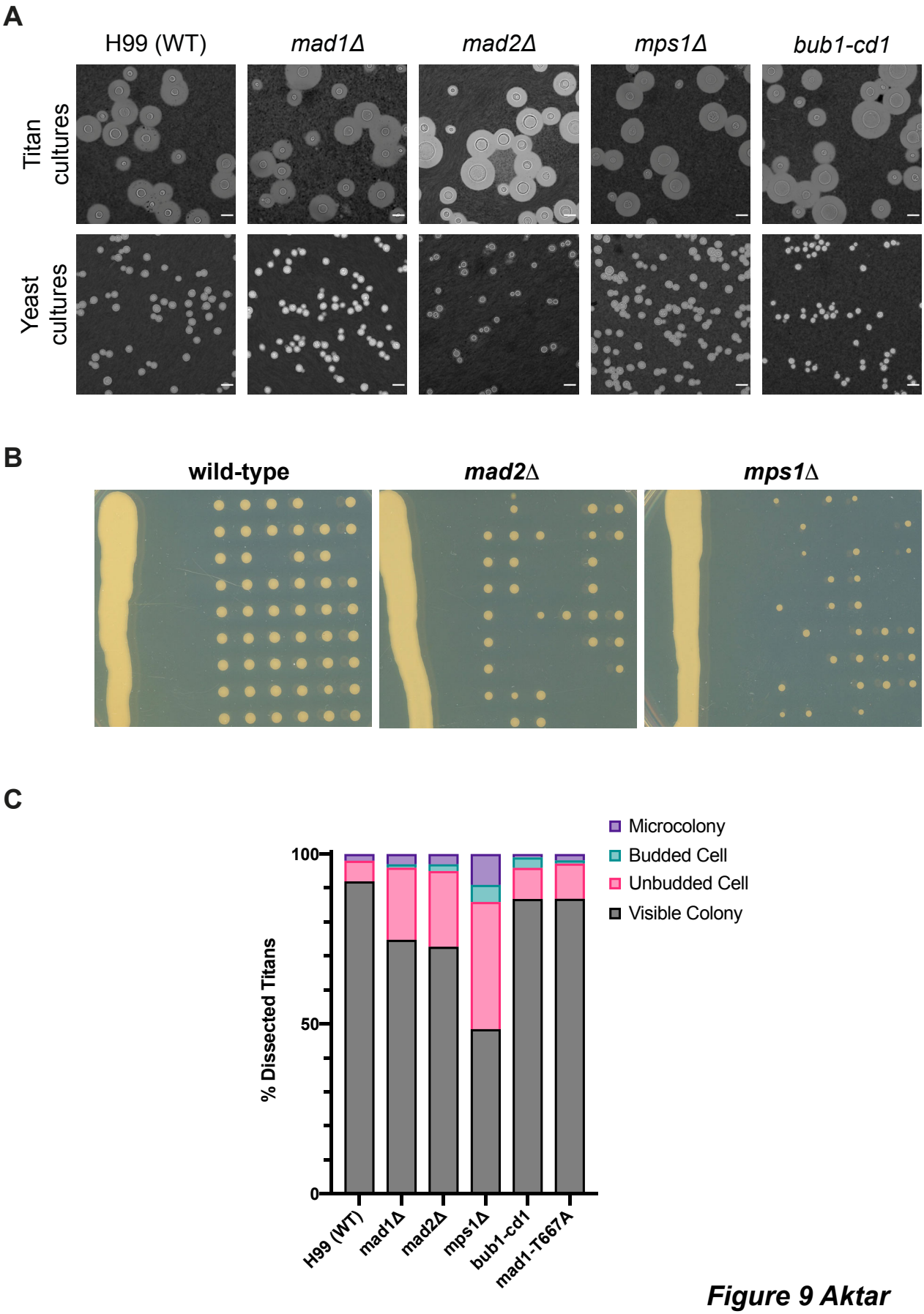

Figure 9 Aktar

Supplementary Figure - Aktar

A ***mad1*Δ PCR confirmation**

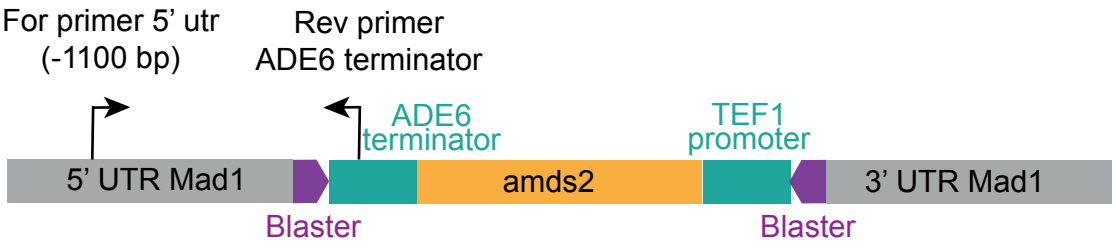

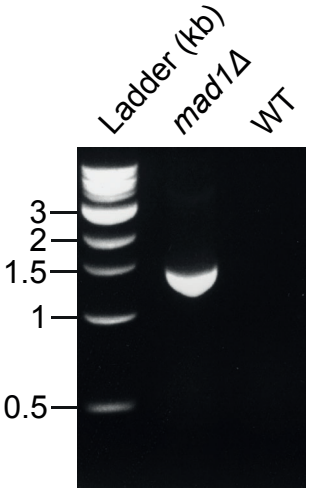

B

Viability (CFU) of *mad1*Δ, *mad2*Δ and *mps1*Δ after nocodazole addition

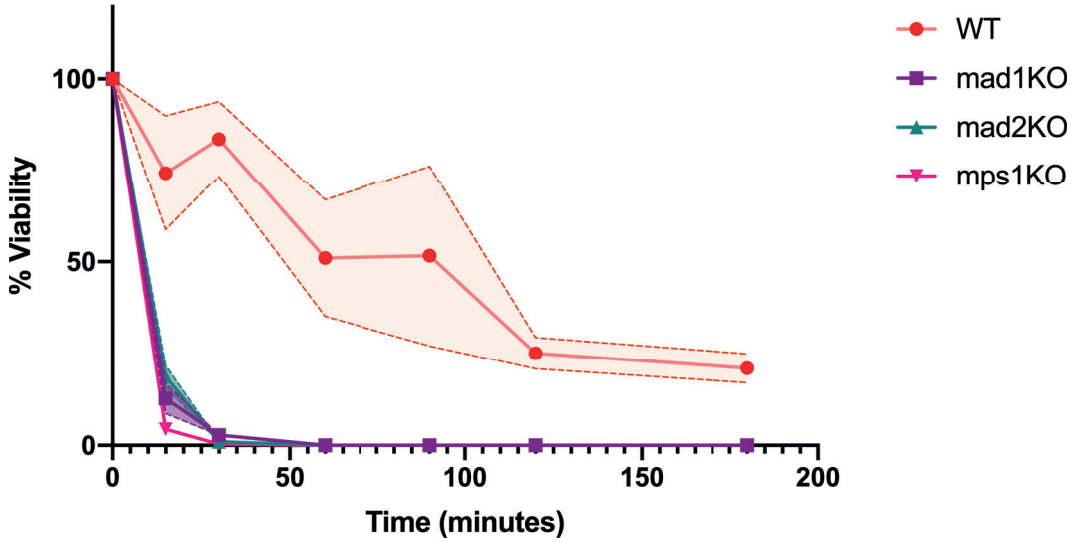

C

***mad1* *567RLK/3A* and *549RLK/3A* phenotypes**